Revision_2

On the *P*-induced behavior of the zeolite phillipsite: an in-situ single-crystal synchrotron X-ray diffraction study

Davide Comboni[1], G. Diego Gatta[1,2*], Paolo Lotti[3], Marco Merlini[1] and Hanns-Peter Liermann[4]

[1]Dipartimento di Scienze della Terra, Università degli Studi di Milano, Via Botticelli 23, I-20133 Milano, Italy

[2] CNR – Istituto di Cristallografia, Sede di Bari, Via G. Amendola 122/O, Bari, Italy

[3]ELETTRA, Sincrotrone Trieste S.c.P.A., Italy, Località Padriciano 99- 34149 Trieste (TS), Italy

[4] DESY, Photon Science, PETRA III, Notkestr. 85, D-22607 Hamburg, Germany

*Corresponding Author:

Phone: +39-02-50315607, Fax: +39-02-50315597, e-mail: diego.gatta@unimi.it

Abstract

The elastic behavior and the structural evolution at high pressure of a natural phillipsite have been investigated by *in situ* single-crystal X-ray diffraction up 9.44 GPa, using a diamond anvil cell and the nominally penetrating *P*-transmitting fluid methanol:ethanol:water (16:3:1) mix. Although no phase transition was observed within the *P*-range investigated, two different compressional regimes occur. Between 0.0001 and 2.0 GPa, the refined elastic parameters, calculated by a second-order Birch-Murnaghan Equation of State (BM-EoS) fit, are V_0 =1005(1) Å^3, K_0= 89(8) GPa for the unit cell volume; a_0= 9.914(7) Å, K_a= 81(12) GPa for the *a*-axis; b_0= 14.201(9) Å, K_b= 50(5) GPa for the *b*-axis and c_0= 8.707(2)Å, K_c= 107(8) GPa for the *c*-axis (K_a: K_b: K_c ~ 1.62:1:2.14). Between 2.0 and 9.4 GPa, a *P*-induced change in the configuration of H_2O molecule, coupled with a change of the tilting mechanisms of the framework tetrahedra, give rise to a second compressional regime, in which the phillipsite structure is softer if compared to the first compressional range. In the second compressional regime, the refined elastic parameter,

calculated by a second-order BM-EoS fit, are V_0 =1098 (7) Å^3, K_0 = 18.8(7) GPa for the unit-cell volume; a_0 = 10.07(3) Å, K_a = 30(2) GPa for the *a*-axis; b_0 = 14.8(1) Å, K_b =11(1) GPa for the *b*-axis and c_0 = 8.94(2) Å, K_c = 21(1) GPa for the *c*-axis (K_a: K_b: K_c~ 2.72:1:1.90). The evolution of the monoclinic β angle with pressure shows two distinct trends in the two compressional regimes: with a negative slope between 0.0001-2.0 GPa, and a positive slope between 2.0-9.4 GPa. The mechanisms, at the atomic scale, that govern the two compressional regimes of the phillipsite structure are described.

Keywords: Phillipsite; high pressure; compressibility; elastic behavior; structure evolution; synchrotron X-ray diffraction.

1. Introduction

Phillipsite is one of the most common natural zeolites with ideal composition $K_2(Na,Ca_{0.5})_3[Al_5Si_{11}O_{32}]\cdot 12H_2O$ (Passaglia and Sheppard 2001), commonly found in altered sediments in "closed" or "open" hydrologic systems, as saline lakes, deep-sea sediments, hot spring deposits, as well as in vugs of basalt and in tuffs (Galli and Loschi Ghittoni1972; Rinaldi et al. 1974; Gottardi and Galli 1985; Armbruster and Gunter 2001). In Langella et al. (2001) is reported how the formation of phillipsite requires low silica activity, along with high pH.

Phillipsite is monoclinc (space group $P2_1/m$, *a* ~9.865 Å, *b* ~14.300 Å, *c* ~8.693 Å, β ~124.92°), with framework density: 15.8 T/1000Å^3 (Baerlocher et al. 2007). In nature, crystals are often found in spherical radiating aggregates, frequently twinned on [001], [021] and [110] (Rinaldi et al. 1974). Several examples of intergrowths with other zeolites (*e.g.*, faujasite, offretite, gismondine, garrionite and gobbinsite) are reported in literature (Rinaldi et al. 1975, Passaglia and Sheppard 2001). In a very recent paper, Danisi et al. (2015) reported coherent twinned intergrowths of merlinoite and phillipsite in a sample originated from Monte Somma, Vesuvius (Italy). The framework of phillipsite (PHI topology, Baerlocher et al. 2007) is built up by four corner-shearing Si/Al tetrahedra, which form four- and eight- membered rings. The four-membered rings (hereafter 4-mRs) and the eight-membered rings (hereafter 8-mRs) are also referred as the secondary building units of PHI framework type (SBU, code 4 and 8 respectively, Baerlocher et al. 2007). In PHI

framework, the 4-mRs are connected to form double cranckshaft chains running parallel to [100]. The PHI framework contains two independent channel systems, running along [100] and [010] (hereafter: 8-mRs[100] and 8-mRs[010] channels, respectively) (Fig. 1). The two sets of channels intersect each other's (Gatta and Lee 2007, Gatta et al. 2009a). The channel running along [100] is confined by two different 8-mRs, hereafter 8-mRs[100]-1 and 8-mRs[100]-2. In the 8-mRs[100]-1, the distance O9-O8 < O7-O7, whereas, in the 8-mRs[100]-2, O9-O8 > O7-O7 (Fig. 1). The double 4-mRs cranckshaft chains form a 8-mRs, here refereed as 8-mRs(001) (Fig. 1). As pointed out by Rinaldi et al. (1974) and Gatta et al. (2009a, 2010, 2015), the Si/Al distribution between the tetrahedral sites is completely disordered in natural phillipsite.

In phillipsite from Richmond, Victoria, Australia (*i.e.*, the same natural species used in this study), the extra-framework population (Fig. 1) is represented by two main cations sites in which Ca (or Na) and K lie. Viewing the structure perpendicular to (010), the Ca-site lies above and below the mirror plane, where the two independent systems of channels intersect. As reported by Gatta et al. (2009a), the coordination shell of Ca site is complex: with a maximum distance of ~ 3 Å, at least 9 mutually excluding configurations are possible. The coordination number (CN) of the Ca sites is 6-7: three oxygen atoms of the tetrahedral framework (O4, O3, O7) and three or four H_2O molecules (among W1, W3, W4-W4', W5, W6). The K site is actually split in two subsites, K1 and K2, only 0.5 Å apart. The two K-sites lie close to the 8-mRs[100] channel wall. If a maximum bond length of 3.4 Å is considered, the CN of both sites is 9 (five oxygen atoms of the framework and four H_2O molecules) (Gatta et al. 2009a). As shown in Gatta et al. (2009a), the H_2O molecules are distributed over 7 independent sites: only W1 and W2 lie on the mirror plane, occupying the *Wyckoff* special position 2*e*; the others sites (*i.e.*, W3, W5, W6, W4, W4' in Gatta et al. 2009a) occupy the general *Wyckoff* position 4*f*. W4 and W4' are two subsites only 0.4 Å apart, and mutually exclusive. The sites W4, W4', W5, W6 occupy central positions in the 8-mRs[010] channel, whereas the W3 site lies close to the channel wall. Among them, W4, W4' and W6 lie at the intersection of the two channels. The W1 and W2 sites lie approximately in the center of the 8-mRs[100] channel (Fig. 1).

The high-temperature behavior of natural and synthetic phillipsites has been object of several investigations (*e.g.*, Steinfink 1962; Stuckenschmidt et al. 1990; Gualtieri et al.1999a, 1999b, 2000; Passaglia et al. 2000; Sani et al. 2002). The thermal behavior, and in particular the dehydration mechanisms, are connected to the nature of the extra-framework population. Due to the lack of single crystals of phillipsite

suitable for non-ambient conditions experiments, Gatta and Lee (2007) investigated the high-pressure behavior of a natural phillipsite powder from Richmond, Victoria, Australia, up to 3.64 GPa, by *in situ* synchrotron X-ray powder diffraction with a diamond anvil cell, using the methanol:ethanol:water = 16:3:1 mix as *P*-transmitting fluid. Axial and volumetric bulk moduli were reported. No unambiguous evidence of phase transition was observed within the *P*-range investigated. Moreover, the quality of the high-*P* powder data, as well as the complex structure of phillipsite, prevented a fulfill discussion about the role played by the extra-framework population on the elastic behavior. Although the general aspects of the high-*P* behavior of the zeolite phillipsite were discussed by Gatta and Lee (2007), a comprehensive characterization of the mechanisms which involve framework and extra-framework population is still missing. In addition, the previous high-*P* study explored a modest *P*-range. In this light, the aim of this work is to reinvestigate the *P*-induced structural evolution of a natural phillipsite (using the sample natural sample previously used by Gatta and Lee 2007) by *in situ* single-crystal synchrotron X-ray diffraction, using a diamond anvil cell.

2. Experimental Methods

The H*P*-synchrotron X-ray single-crystal diffraction experiments were conducted at the Extreme Conditions Beamline P02.2 at PETRA-III/DESY, Hamburg, Germany. Data collections were performed with an incident beam of 42.7 keV in energy, and a focusing spot of ~8.5 (H) μm x 1.8 (V) μm originated from a compound refractive lenses system, consisting of 121 Be lenses with a radius of 50 μm (400 μm beam acceptance) and a focal length of 1221 mm. A single crystal of phillipsite (~50x50x20 μm), free of twinning under polarized-light microscope and with lamellar morphology, was selected for the experiment. The crystal was loaded in a symmetric DAC equipped with Boehler-Almax design diamonds/seats with a 70° opening and 300 μm culets size. A 250-μm-thick foil of stainless steel was used as gasket, which was pre-indented to ~60 μm and then drilled with a hole of ~200 μm in diameter, using a spark-erosion device. A few ruby spheres were added into the gasket hole for *P*-measurement, by the ruby-fluorescence method (Mao et al. 1986; pressure uncertainty ± 0.05 GPa). The mix methanol:ethanol:water = 16:3:1 (hereafter *m.e.w.*) was used as hydrostatic *P*-transmitting fluid (Angel et al. 2007). This pressure medium is considered potentially "*penetrating*" (Gatta and Lee 2014), as at least the molecules of H_2O (∅ ~ 2.65Å) and CH_3OH (∅ ~ 3.76 Å) may theoretically be incorporated into the 8-mRs[100] channels of phillipsite (∅ ~ 3.8 Å, Baerlocher et al.

2007). Pressure was increased (up to P_{max} = 9.4 GPa, Table 1) with an automated pressure-driven system from Sanchez Technology (Viarmes, France) and measured with the online ruby/alignment system powered by a 100 mW 458-nm laser. Diffraction images were collected with a Perkin Elmer XRD 1621 flat panel detector, using an in-house script for collecting step-scan diffraction images. The sample to detector distance (402.34 mm) was calibrated using a CeO_2 standard (NIST 674a). A few data collections were performed in decompression (Table 1). The diffraction images were then converted to conform to the "Esperanto" format of the program CrysAlis (Agilent 2012; Rothkirch et al. 2013). At all pressure points, the adopted data collection strategy consisted in a pure ω-scan (-28°≤ ω ≤ +28°), with a step size of 1° and an exposure time of 1 s/frame; then Bragg peaks were indexed. Intensities of the diffraction peaks were integrated and corrected for Lorentz-polarization effects, using the CrysAlis package (Agilent 2012). Corrections for adsorption (due to the DAC components) was applied by the semi-empirical *ABSPACK* routine implemented in CrysAlis. The refined unit-cell parameters are listed in Table 1.

3. Structure refinement protocol

All the structure refinements, at different pressures, were performed using the software JANA2006 (Petříček et al. 2014) in the space group $P2_1/m$, as suggested by the reflection conditions. Reflections were "observed" down to an interplanar distance $d \sim 0.8$ Å. At $P \geq 2.57$ GPa, it was observed an abrupt decrease in the number of observed reflections, with a consequent increase of the R_1 factor (Table 2, deposited). The isotropic structure refinements were possible up to 4.85 GPa ($P11$). For the first refinement ($P1$, 0.2 GPa), the input fractional coordinates of the framework sites were taken from Gatta et al. (2009a). The positions of the extra-framework sites were obtained by a careful analysis of the difference-Fourier maps of the electron density. At $P1$, one Ca site and two mutually independent K sites were identified, along with six independent sites assigned to the H_2O molecules, according to the structure model of Gatta et al. (2009a); the same sites labeling scheme was used (*i.e.*, Ca, K1, K2 and W1-6, Table 3, deposited). Briefly, W1 and W2 sites lie in the center of 8-mRs[100]-1 and 8-mRs[100]-2, respectively, whereas W3 and W5 occupy the 8-mRs[010] channel; the W4 and W6 sites lie at the intersection of the two channel systems. As the analysis of the difference-Fourier maps revealed only one strong peak lying on the mirror plane between the position of the

143 sites W4-W4' in Gatta et al. (2009a), in the structure model of this study we refined only one site (labelled as
144 W4, Table 3). No specific restrains were applied to the Ca site, whereas the K1-K2 sites were refined with
145 the same displacing parameter (DP). The same restriction was applied to all the H_2O sites. This protocol was
146 used in all the refinements at different pressures, with the following exceptions:
147 - The DPs of the H_2O sites were forced to have an U_{iso} value fixed to 0.075 $Å^2$. This value is arbitrary,
148 although very reasonable: the refined U_{iso} of H_2O sites at *P*1 was ~0.079(4)$Å^2$ (Table 3).
149 - The occupancy of the Ca site was fixed to the one obtained from the refinement of *P*1. The sum of
150 the K1 and K2 site occupancies, in all the refinements at $P > P1$, were forced to assume the value found at
151 *P*1.
152 - The R_1 factors were all ≤ 10% up to 2.56 GPa (*P*8). At $P > P8$, the R_1 values increased significantly;
153 the last refinement which reached convergence is that at 4.85 GPa (*P*11). At $P > P8$, the occupancy of the
154 H_2O sites showed an anomalous increase. As the adsorption of H_2O molecule at this pressure is not realistic
155 (*i.e.*, all the previous experimental findings available in literature reported *P*-induced over-hydration effects
156 at $P<1$ GPa, Gatta and Lee 2014 for a review), we introduced a further restrain: the *sum* of the H_2O site
157 occupancies was fixed to the value obtained by the refinement at *P*8 (*i.e.*, 14.36±1.16 molecules per formula
158 unit, m.p.f.u.). The sum at *P*8 is equal, within 1σ, to that obtained at *P*1 (*i.e.*, 14.00±0.84 m.p.f.u.).
159 For all the structure refinements, Table 2 lists the principal statistical parameters. Site coordinates and
160 occupancies are given in Table 3 (deposited). Refined bond distances are reported in Tables 4 and 5
161 (deposited). Other relevant structural parameters are reported in Table 6, 7, 8, 9.
162
163 ## 4. Results
164 ### 4.1 High-pressure elastic behavior
165 The unit-cell parameters at eighteen *P*-points up to 9.44(5) GPa, and three points in decompression, are
166 reported in Table 1. The *P*-induced evolution of the unit-cell parameters is shown in Fig. 2. The evolution of
167 the unit-cell parameters show at least two different compressional regimes. From *P*1 to *P*6 (1.82 GPa),
168 phillipsite is stiffer than in the second regime [*i.e.*, from *P*9 (3.13 GPa) to *P*19 (9.44 GPa)]. Up to *P*8 (2.56
169 GPa), the value of the β angle decreases, whereas at $P \geq P9$ there is a clear inversion of the trend (Fig. 2).
170 The evolution of the β angle is diagnostic for the change of the compressional regimes. For the two regimes,

a Birch-Murnaghan Equation of State truncated to the second order was fitted to the experimental *P*-*V* data using the *EoSFit 7.0* software (Angel et al. 2000, 2014). We did not consider the unit-cell parameters of *P*7 (2.14 GPa) and *P*8 in the calculation of the elastic parameters, considering the *P*-range between *P*7 and *P*8 as a transitional interval between the two regimes. The refined elastic parameters are reported in Table 10. Bulk moduli K_V , K_a , K_b , K_c of the first regime (hereafter named K_x^1), are significantly higher than the ones obtained for the second regime (hereafter named K_x^2), suggesting that, at low pressure, phillipsite is "stiffer". In the second regime, the linear bulk moduli decrease drastically and anisotropically (*e.g.*, K_a decreases by about 2.5 times, whereas K_b and K_c decrease by about 5 times). The reasons of such changes of the elastic behavior, at the atomic level, will be discussed in the next sessions.

4.2 Pressure-induced structural evolution: deformation of the Si/Al framework

The intra-tetrahedral T-O distances (reported in Table 4) do not show drastic changes within the *P*-range investigated. The most significant changes of the inter-tetrahedral angles are those observed for the T1-O7-T3, T2-O8-T2, T4-O6-T2, and T4-O1-T3 angles, reported in Table 11. Fig. 3 shows the trends of these T-O-T angles (normalized to the value at *P*1). At *P*7, all trends change markedly. The inter-tetrahedral tilting gives rise to a pronounced increase of the ellipcity of all the 8-mRs. In order to explain the behavior of the 8-mRs, we introduce the ε parameter (*i.e.*, the ellipticity ratio) as the *b/a* ratio, where *b* is the minor and *a* the major axis of any given ring (*e.g.*, Gatta and Lee 2007; Gatta et al. 2009a). The ε-ratio for the 8-mRs[100]-1 (hereafter $\varepsilon_{8\text{-mRs}[100]\text{-}1}$) is defined as O9-O8/O7-O7 (with O7-O7>O9-O8); for the 8-mRs[100]-2, the ε-ratio (hereafter $\varepsilon_{8\text{-mRs}[100]\text{-}2}$) is defined as O7-O7/O9-O8 (as O7-O7<O9-O8). For the 8-mRs[010] and the 8-mRs(001) (hereafter $\varepsilon_{8\text{-mRs}[010]}$ and $\varepsilon_{8\text{-mRs}(001)}$), the ε ratios are defined as O3-O3/O1-O1 and O9-O8/O5-O5, respectively. The trend of all the ε values of the 8-mRs are shown in Fig. 4. Every ring tends to increase its ellipticity with the pressure increase, as previously observed in several others zeolites (*e.g.* Gatta et al. 2005, 2009b; Lotti et al. 2016). Contrarily to what observed by Gatta et al. (2007), the ε ratio of the 8-mRs[100]-2 is more pronounced than that of the 8mRs[100]-1 one. This feature is maintained at high-*P* and, interestingly, the trends of $\varepsilon_{8\text{-mRs}[100]\text{-}1}$, $\varepsilon_{8\text{-mRs}[100]\text{-}2}$ and $\varepsilon_{8\text{-mRs}[010]}$ are practically parallel (Fig. 4). However, at a careful analysis from *P*7 to *P*11, $\varepsilon_{8\text{-mRs}[100]\text{-}2}$ decreases more pronouncedly than $\varepsilon_{8\text{-mRs}[100]\text{-}1}$ and $\varepsilon_{8\text{-mRs}[010]}$. In fact, in the considered *P*-range, the slope of $\varepsilon_{8\text{-mRs}[100]\text{-}2}$ is -0.059(2), whereas the slope of both $\varepsilon_{8\text{-mRs}[100]\text{-}1}$ and

199 $\varepsilon_{8\text{-mRs}[010]}$ is -0.052(3): the 8-mRs[100]-2 is, therefore, more affected by the *P*-induced deformation than 8-
200 mRs[100]-1 and 8-mRs[010].

201 If the normalized O3-O3 and O7-O7 diameters of the 8-mRs[010] are plotted *vs. P*, the trend are
202 almost parallel up to *P*7 (Fig 5). At $P > P7$, the diameter O3-O3 begins to decrease abruptly, whereas O7-O7
203 slightly increases. As the diameter O7-O7 is parallel to [100] and O3-O3 almost parallel to [001], this can
204 explain the observed $K_a > K_c$ at $P > P7$ (Table 10).

205 It is also interesting to note that at *P*8 the β angle reverses its negative trend with *P,* and begins to
206 increase. The change of β is somehow related to some T-O-T angles. We expect that the evolution of β might
207 depend on the evolution of the inter-tetrahedral angles of the 8-mRs[010], and in particular on a combination
208 of the T3-O1-T4 and T2-O6-T4 angles (Fig. 1). More in detail, if T3-O1-T4 and T2-O6-T4 were lying on the
209 same plane (perpendicular to [010]), at an increase of their values would correspond a decrease of β. They
210 actually do not lie on the same plane; however, if the value of the difference [(T2-O6-T4)-(T3-O1-T4)] is
211 plotted *vs.* pressure (Fig. 6), an almost overlapped trend to that of β is observed. This finding suggests that
212 the combined effect of the T3-O1-T4 and T2-O6-T4 angles evolution can play a role in the evolution of the β
213 angle, and thus on the distortion of the (monoclinic) unit-cell.
214

215 **4.3 Pressure-induced structural evolution: evolution of the extra-framework population**

216 *4.3.1 W sites*

217 The first changes in the evolution of the extra-framework population are already observed at low-*P*
218 regime. At *P*2, the analysis of the difference-Fourier maps of the electron density showed the presence of a
219 maximum close (but distinct) to the position of W2. This peak, labelled as W2' in this study, was not found
220 in the analysis of the difference-Fourier maps at *P*1. Although we cannot exclude that the occupancies of the
221 H_2O sites are influenced by the constrains adopted for the DP values, it is possible that the sum of the
222 occupancies of W2 and W2' (which are mutually exclusive) at *P*2 is equal, within the *e.s.d.*, to the
223 occupancy of W2 site at *P*1. The distances W2'-O8 (*i.e.*, 2.878(3) Å) and W2'-O2 (*i.e.*, 2.893(3) Å) at *P*2 are
224 shorter than the distances W2-O8 (*i.e.*, 3.205(3) Å) and W2-O2 (*i.e.*, 3.076(3) Å), and this suggests that the
225 new W2' site is involved in an energetically more favorable H-bonding network if compared to W2. At *P*9,
226 the two maxima ascribable to W2 and W2' were not distinctly observed anymore: only one distinct electron-

density peak was found. As the distance between the two subsites decreases significantly from *P*6 to *P*8 (from ~1 Å to ~0.75 Å, respectively), it is highly likely that they converge to one site at *P*9 (3.13 GPa), here re-labelled as W2 (Table 3, Fig. 7). It is worth to point out that the occupancy of W2 at *P*9 is slightly lower than the sum of the W2 and W2' sites at *P*8 (Table 3).

As pressure increases, the distance between W1 and Ca decreases (Table 5), toward non-realistic values expected for a Ca-W distance (Fig. 7). This finding suggests that Ca and W1 are actually two mutually exclusive sites, even in the low-*P* regime. An additional finding concerns the "migration" of W1 out of the 8-mRs[100]-1. Such a behaviour implies a change of its H-bonding scheme. As reported in Table 5, at *P*1 the distance W1-O9 and W1-O3 are 2.940(3) and 3.081(3)Å, respectively. The same distances at *P*11 are 2.690(3) and 3.229(3) Å, respectively, which means that the distance W1-O9 decreases by ~ 9%, whereas the W1-O3 increases by ~4.5%.

The analysis of the difference-Fourier maps, based on the refinements at *P*10 and *P*11, revealed the presence of two new maxima, here labeled as W2'' and W1', lying in the 8-mRs[100]-2 and 8-mRs[100]-1 rings, respectively (Table 3, Fig. 7), with partial site occupancy and mutually exclusive with the co-respective W1 and W2 (Table 3). These new sites have distances with some framework oxygen sites ascribable to H-bond interactions (*e.g.*, W1'-O9 ~ 2.9 Å, W2''-O8 ~2.5 Å, W2''-O2 ~2.6 Å).

Additional effects of H_2O migration among the W sites are observed at W4, W5 and W6. The fractional coordinates of the W3, W5 and W6 sites do not show any substantial change with the increase of pressure. The occupancy of the W4 sites decreases as pressure rises, whereas the occupancies of W5 and W6 increase. At $P > P9$, no evidence of the W4 site was found in the difference-Fourier maps, coupled with significantly higher densities at W5 and W6 than those observed at *P*1 (Fig. 8).

A general view of the *P*-induced changes involving the extra-framework population is shown in Fig. 7.

4.3.2 Ca and K1-K2 sites

As reported in Table 5, the distance Ca-O7 increases with pressure, whereas the distances Ca-O4 and Ca-O3 decrease. This trend leads the Ca site toward the mirror plane located at $y = ¼$. This behavior might

be correlated to the tilting of the TO_4 tetrahedra and, in particular, to the closure of the O4-O7-O3 angle in the 8-mRs[100]-1.

The structural data show also a correlation between the distances K1/K2-O1 and K1/K2-O8 and the inter-tetrahedral angles T3-O1-T4 and T2-O8-T2, respectively. As explained in the previous section, the principal effect of the hydrostatic compression on the 8-mRs(001) is the tilting of the TO_4 tetrahedra, which leads to a reduction of the T3-O1-T4 and T2-O8-T2 angles with pressure. The decrease of the aforementioned angles leads to a shortening of the K1/K2-O1 and K1/K2-O8 distances (Table 5).

5. Discussion and conclusions

This is the first experiment in which the high-*P* behavior of a natural phillipsite is described on the basis of single-crystal X-ray diffraction data (collected up to 9.4 GPa). The previous experiment on phillipsite was conducted on a polycrystalline sample up to 3.6 GPa (Gatta and Lee 2007). Gatta and Lee (2007) described the elastic behavior of phillipsite on the basis of powder data. However, the low quality of the powder data themselves, along with the modest *P*-range investigated (*i.e.*, P_{max} = 3.6 GPa), did not allow the authors to have a clear picture of the high-*P* behavior of this zeolite, and only one BM-EoS was used to model its compressibility. A potential change of the compressional behavior was already reported by Gatta and Lee (2007) at $P > 2$ GPa. In this study, we used the same natural sample previously used by Gatta and Lee (2007). In this light, this work can be considered as an extension of the first study. Also in this case, we observe a change of the compressional behavior of phillipsite between 2.0-2.5 GPa, which is not due by a potential penetration of the *P*-fluid molecules. The inversion of β-trend is likely the most evident effect of such a change. The diffraction patterns and the structure refinements confirmed that the $P2_1/m$ is preserved within the entire *P*-range investigated (*i.e.*, 0 – 9.4 GPa). Therefore, the change of the elastic behavior does not reflect a phase transition, but rather a change of the deformation mechanisms at the atomic scale.

More specifically, phillipsite experiences a "softening" at $P > 2$-2.5 GPa, and the bulk modulus in the low-*P* regime is drastically higher than that of the high-*P* regime (*i.e.*, 89(8) *vs.* 18.8(7) GPa, Table 10). A similar behavior was previously observed in other open-framework materials (*e.g.*, Gatta et al. 2006, 2008, 2009b, 2012). As the tetrahedra behave as rigid units (at least at a first approximation), the structure deformation is basically governed by tetrahedral tilting and by the rearrangement of the extra-framework

population, as usually observed in zeolites (*e.g.*, Gatta 2008, Gatta and Lee 2014, Gatta et al. 2014, Lotti et al. 2016).

The elastic anisotropic scheme of phillipsite is preserved within the *P*-range investigated, with $K_a > K_c > K_b$. The structure is, therefore, more compressible along [010]. From the low- to the high-*P* regime, the linearized bulk modulus K_b decreases from 50(5) to 12(1) GPa. Such a behavior might be somehow influenced by a change of the extra-framework population and, more specifically, by the disappearance of the W4 site. W4 (along with W5 and W6) lies almost in the center of the 8-mRs[010] channel, in such a way that a helicoidally H_2O-chain occurs. The lack of W4 implies a reduced "pillar effect" of the H_2O-chain (Fig. 7 and 8). As the H_2O-chain is perpendicular to (010), its weakening does not affect significantly the compressibility along [100] or [001]. However, if the ratio O7-O7/O3-O3 is plotted vs. *P*, where O3-O3 and O7-O7 are two independent diameters of the 8-mRs[010] channel, we observe an almost horizontal trend up to $P7$ and then a drastic increase at $P > P7$ (Fig. 5). Therefore, one of the reasons of the softening along [100] and [001] can be ascribed to the tilting of the 8-mRs[010]-tetrahedra, in response to the disappearance of W4. The tilting causes the deformation of the 8-mRs[010] channel and, in turn, the β-inversion (as described in the section 4.2).

An additional cause of the elastic anisotropy may be correlated to the migration of W1. The lack of W1 at high-*P*, in the 8-mRs[100]-1, leads to a significant shortening of the O8-O9 diameter, which is perpendicular to [001]. Therefore, the migration of W1 cannot affect K_a or K_b but only K_c.

There is not a unique explanation about the H_2O sites migration at high pressure and the occurrence of subsites, *e.g.* W1', W2', W2'' (Table 3), as described in the section 4.3.1. The lack of the proton positions does not allow a clear view of the H-bonding network. However, it appears that the framework deformation leads to energetically most favorable H-bonding connection with H_2O molecules located in a slightly different positions than the parent ones (at room conditions), promoting split and, in general, H_2O sites migration.

6. Acknowledgments

The authors acknowledge the Italian Ministry of Education, MIUR-Project: "Futuro in Ricerca 2012 - ImPACT- RBFR12CLQD". DESY – PETRA III (Hamburg) is thanked for the allocation of beamtime. Y.

Lee is thanked for the sample of phillipsite from Richmond, Victoria, Australia. Two anonymous reviewers are thanked for their constructive suggestions.

7. References

Agilent (2012) Chrysalis RED, Agilent Technologies Ltd, Yarnton.

Angel RJ, Hazen RM, Downs RT (2000) High-Temperature and High-Pressure Crystal Chemistry. Rev Mineral Geochem 41: 35-60.

Angel RJ, Bujak M, Zhao J, Gatta GD, Jacobsen SD (2007) Effective hydrostatic limits of pressure media for high-pressure crystallographic studies. J Appl Crystallogr 40:26-32.

Angel RJ, Alvaro M, Gonzalez-Platas J (2014) EosFit7c and a Fortran module (library) for equation of state calculations. Z Kristallogr 229:405-419.

Armbruster T, Gunter ME (2001) Crystal Structures of Natural Zeolites. Rev Mineral Geochem 45:1-57.

Baerlocher C, McCusker LB, Olson DH (2007) Atlas of Zeolite Framework Types, sixth ed., Elsevier, Amsterdam.

Danisi RM, Armbruster T, and Nagashima M (2015) Structural intergrowth of merlinoite/phillipsite and its temperature-dependent dehydration behaviour: a single-crystal X-ray study. Mineral Mag 79:191-203.

Galli E, Loschi Ghittoni A.G (1972) The crystal chemistry of phillipsites. Am Mineral 57:1125–1145.

Gatta GD, Comodi P, Zanazzi PF, Ballaran TB (2005) Anomalous elastic behavior and high-pressure structural evolution of zeolite levyne. Am Mineral 90:645-652.

Gatta GD, Nestola F, Boffa Ballaran T (2006) Elastic behavior, phase transition and pressure induced structural evolution of analcime. Am Mineral 91:568-578.

Gatta GD, Lee Y (2007) Anisotropic elastic behaviour and structural evolution of zeolite phillipsite at high pressure: A synchrotron powder diffraction study. Microp Mesop Mater 105:239–250.

Gatta GD, Rotiroti N, Boffa Ballaran T, Pavese A (2008) Leucite at high-pressure: elastic behaviour, phase stability and petrological implications. Am Mineral 93:1588-1596.

Gatta GD, Cappelletti P, Rotiroti N, Slebodnick C, Rinaldi R (2009a) New insights into the crystal structure and crystal chemistry of the zeolite phillipsite. Am Mineral 94:190–199.

Gatta GD, Rotiroti N, Boffa Ballaran T, Sanchez-Valle C, Pavese A (2009b) Elastic behavior and phase stability of pollucite, a potential host for nuclear waste. Am Mineral 94:1137-1143.

Gatta GD, Cappelletti P, Langella A (2010) Crystal-chemistry of phillipsites from the Neapolitan Yellow Tuff. Eur J Mineral 22:779-786.

Gatta GD, Lotti P, Nestola F and Pasqual D (2012) On the high-pressure behavior of gobbinsite, the natural counterpart of the synthetic zeolite Na-P2. Microp Mesop Mater 163:259-269.

Gatta GD, Comboni D, Alvaro M, Lotti P, Càmara F, Domeneghetti MC (2014) Thermoelastic behavior and dehydration process of cancrinite. Phys Chem Minerals 41:373–386.

Gatta GD, Lee Y (2014) Zeolites at high pressure: A review. Mineral Mag 78: 267-291.

Gatta GD, Cappelletti P, de' Gennaro B, Rotiroti N, Langella A (2015) New data on Cu-exchanged phillipsite: a multi-methodological study. Phys Chem Minerals 42:723-733.

Gottardi G, Galli E (1985) Natural zeolites. Minerals and rocks series. Springer-Verlag, p. 409.

Langella A, Cappelletti P, de' Gennaro R (2001) Zeolites in closed hydrologic systems. Rev Mineral Geochem 45:235-260.

Gualtieri AF, Caputo D, Colella C (1999a) Ion-exchange selectivity of phillipsite for Cs+: a structural investigation using the Rietveld method. Microp Mesop Mater 32:319–329.

Gualtieri AF, Passaglia E, Galli E, Viani A (1999b) Rietveld structure refinement of Sr-exchanged phillipsites. Microp Mesop Mater 31:33–43.

Gualtieri AF, Passaglia E, Galli E (2000) Rietveld structure refinement of natural and Na-, K-, Ca-, and Ba-exchanged phillipsites. In: Colella C, Mumpton FA (eds) Natural zeolites for the third millennium. De Frede, Naples, pp. 93–110.

Lotti P, Gatta DG, Comboni D, Merlini M, Pastero L, Hanfland M (2016) AlPO4-5 zeolite at high pressure: Crystal–fluid interaction and elastic behaviour. Microp Mesop Mater 228:158-16.

Mao HK, Xu J, Bell PM (1986) Calibration of the ruby pressure gauge to 800-kbar under quasi-hydrostatic conditions. J Geophys Res 91:4673-4676.

Passaglia E, Galli E, Gualtieri AF (2000) Natural Zeolites for the Third Millennium, De Frede, Naples, 259–267.

Passaglia E, Sheppard RA (2001) The crystal chemistry of zeolites. Rev Mineral Geochem 45:69–116.

Petříček V, Dušek M, Palatinus L (2014) Crystallographic Computing System JANA2006: General features. Z Kristallogr 229: 345–352.

Rinaldi R, Pluth JL, Smith JV (1974) Zeolites of the phillipsite family. Refinement of the crystal structure of phillipsite and harmotome. Acta Crystallogr B30:2426–2433.

Rinaldi R, Smith JV, Jung G (1975) Chemistry and paragenesis of faujasite, phillipsite, and offretite from Sasbach, Kaiserstuhl, Germany. Neues Jahrb Mineral Monat 10: 433–443.

Rothkirch A, Gatta GD, Meyer M, Merkel S, Merlini M, Liermann H-P (2013) Single-crystal diffraction at the Extreme Conditions beamline P02.2: procedure for collecting and analyzing high-pressure single-crystal data. J Synchrotron Rad 20:711-720.

Sani A, Cruciani G, Gualtieri AF (2002) Dehydration dynamics of Ba-phillipsite: an in situ synchrotron powder diffraction study. Phys Chem Minerals 29:351-361.

Steinfink H (1962) The crystal structure of the zeolite phillipsite. Acta Crystallogr 15:644–651.

Stuckenschmidt E, Fuess H, Kvick A (1990) Investigation of the structure of harmotome by X-ray (293 K, 100 K) and neutron-diffraction (15 K). Eur J Mineral 2:861-874.

Table 1. Unit-cell parameters of the zeolite phillipsite with *P*. $P_{19\text{-}21}$ in decompression.

P_n	*P*(GPa)	*V* ($Å^3$)	*a*(Å)	*b*(Å)	*c*(Å)	*β*(°)
P_1	0.20(5)	1001.6(3)	9.8934(4)	14.184(2)	8.6998(3)	124.874(6)
P_2	0.60(5)	1000.2(3)	9.8982(4)	14.153(2)	8.6941(4)	124.792(7)
P_3	0.94(5)	993.8(3)	9.8780(4)	14.105(2)	8.6790(4)	124.733(7)
P_4	1.22(5)	991.1(3)	9.8675(4)	14.082(2)	8.6739(4)	124.683(7)
P_{4b}	1.22(5)	991.6(3)	9.8689(4)	14.085(2)	8.6756(4)	124.685(6)
P_5	1.60(5)	988.8(3)	9.8546(5)	14.068(2)	8.6681(5)	124.631(8)
P_6	1.82(5)	985.3(3)	9.8402(4)	14.051(2)	8.6585(4)	124.612(7)
P_7	2.14(5)	973.4(3)	9.7930(4)	13.995(2)	8.6242(4)	124.560(6)
P_8	2.57(5)	965.2(3)	9.7643(4)	13.952(2)	8.6013(4)	124.539(7)
P_9	3.13(5)	956.9(3)	9.7536(5)	13.886(3)	8.5839(5)	124.610(8)
P_{10}	3.92(5)	941.8(3)	9.7283(7)	13.782(4)	8.5434(8)	124.70(1)
P_{11}	4.85(5)	913.0(3)	9.6822(9)	13.569(4)	8.468(1)	124.85(2)
P_{12}	5.26(5)	900.4(5)	9.6498(9)	13.490(4)	8.432(1)	124.88(2)
P_{13}	6.14(5)	881.0(3)	9.5903(7)	13.379(4)	8.3692(8)	124.88(1)
P_{14}	6.71(5)	864.6(3)	9.5410(9)	13.279(4)	8.323(1)	124.93(2)
P_{15}	7.48(5)	853.8(3)	9.514(1)	13.203(5)	8.300(1)	125.02(2)
P_{16}	8.20(5)	841.7(3)	9.477(1)	13.137(6)	8.264(1)	125.11(2)
P_{17}	8.73(5)	829.6(4)	9.435(2)	13.092(7)	8.220(2)	125.20(3)
P_{18}	9.44(5)	821.1(4)	9.393(2)	13.084(8)	8.187(2)	125.31(3)
P_{19}	1.93(5)	989.8(3)	9.8283(7)	14.103(3)	8.6691(5)	124.539(9)
P_{20}	1.93(5)	971.9(3)	9.7718(5)	14.008(2)	8.6196(4)	124.537(7)
P_{21}	0.50(5)	1007.9(4)	9.925(1)	14.181(5)	8.730(1)	124.88(2)

Table 2 (deposited). Details pertaining to the structure refinements of phillipsite at different pressures.

	P_1 0.20 GPa	P_2 0.60 GPa	P_3 0.94 GPa	P_4 1.22 GPa	P_5 1.60 GPa	P_6 1.82 GPa	P_7 2.14 GPa
min≤h≤max	-16; 16	-15; 15	-16; 15	-16; 15	-16; 15	-16; 15	-15; 15
min≤k≤max	-10; 10	-10; 12	-10; 11	-11; 11	-11; 11	-10; 11	-11; 11
min≤l≤max	-13; 12	-14; 14	-14; 14	-13; 14	-13; 14	-13; 14	-13; 14
Unique reflections	1934	1999	1860	1841	1839	1812	1823
Observed reflections $I > 3\sigma(I)$	1181	1500	1395	1360	1356	1312	1349
Number of refined parameters	82	84	84	84	84	83	84
Number of restrains	2	1	1	1	1	1	1
R_{int} (obs)	0.067	0.078	0.078	0.084	0.081	0.083	0.089
R_{int} (all)	0.080	0.088	0.087	0.092	0.091	0.093	0.097
R_1 (obs)	0.0224	0.0232	0.0250	0.0269	0.0253	0.0278	0.0229
R_1 (all)	0.0255	0.0244	0.0261	0.0279	0.0262	0.0289	0.0240
wR_1 (obs)	0.0803	0.0928	0.0907	0.0974	0.0955	0.0980	0.1063
wR_1 (all)	0.0809	0.0945	0.0911	0.0978	0.0960	0.0985	0.1067
Residuals (e^-/Å^3)	+0.23; -0.17	+0.22; -0.24	+0.25; -0.26	+0.24; -0.28	+0.19; -0.19	+0.22; -0.23	+0.20; -0.23

	P_8 2.57 GPa	$P_9$3.13 GPa	P_{10} 3.92 GPa	P_{11} 4.85 GPa	P_{21} 0.50 *GPa*
min≤h≤max	-15; 16	-15; 15	-15; 15	-15; 14	-13; 10
min≤k≤max	-10; 11	-10; 11	-9; 10	-9; 10	-11; 8
min≤l≤max	-13; 14	-12; 14	-11; 13	-11; 13	-8; 14
Unique reflections	1803	1762	1888	1559	1884
Observed reflections $I > 3\sigma(I)$	1297	1232	1022	813	1154
Number of refined parameters	83	84	83	83	80
Number of restrains	1	2	2	2	1
R_{int} (obs)	0.102	0.114	0.130	0.162	0.090
R_{int} (all)	0.110	0.126	0.153	0.192	0.010
R_1 (obs)	0.0718	0.0444	0.0392	0.0570	0.0826
R_1 (all)	0.0729	0.0457	0.0440	0.0612	0.0862
wR_1 (obs)	0.1167	0.1297	0.1458	0.1673	0.1027
wR_1 (all)	0.1174	0.1303	0.1469	0.1685	0.1033
Residuals(e^-/Å^3)	+0.26; -0.27	+0.29; -0.25	+0.21; -0.23	+0.34; -0.33	+0.29; -0.23

Table 3 (deposited). Refined positional and displacement parameters of phillipsite at different pressures. (*) fixed value ;(**) value refined with a restrain.

Site	*P* (GPa)	*s.o.f.*	*x*	*y*	*z*	U_{iso} (Å^2)
Ca	P_1(0.20)	0.31(1)	0.6672(9)	0.372(1)	0.562(1)	0.041(4)
	P_2(0.60)	0.308*	0.674(1)	0.370(1)	0.572(1)	0.048(2)
	P_3(0.94)	0.308*	0.678(1)	0.367(1)	0.574(1)	0.048(2)
	P_4(1.22)	0.308*	0.681(1)	0.365(1)	0.575(1)	0.049(2)
	P_5(1.60)	0.308*	0.684(1)	0.362(1)	0.577(1)	0.049(2)
	P_6(1.82)	0.308*	0.685(1)	0.362(1)	0.577(1)	0.050(2)
	P_7(2.14)	0.308*	0.687(1)	0.360(1)	0.578(1)	0.047(2)
	P_8(2.57)	0.308*	0.687(1)	0.359(1)	0.577(1)	0.042(2)
	P_9(3.13)	0.308*	0.690(2)	0.356(2)	0.577(2)	0.055(3)
	P_{10}(3.92)	0.308*	0.682(2)	0.357(3)	0.576(3)	0.075(5)
	P_{11}(4.85)	0.308*	0.684(4)	0.361(5)	0.580(5)	0.12(1)
	P_{21}(0.50)	0.308*	0.669(1)	0.367(1)	0.566(1)	0.060(3)
T1(Si)	P_1(0.20)	1.00	0.7264(3)	0.0073(3)	0.2855(3)	0.0139(6)
	P_2(0.60)	1.00	0.7256(2)	0.0068(3)	0.2861(3)	0.0113(6)
	P_3(0.94)	1.00	0.7254(2)	0.0073(3)	0.2863(3)	0.0112(6)
	P_4(1.22)	1.00	0.7250(3)	0.0074(3)	0.2865(3)	0.0114(6)
	P_5(1.60)	1.00	0.7249(2)	0.0073(3)	0.2870(3)	0.0127(6)
	P_6(1.82)	1.00	0.7246(3)	0.0071(3)	0.2867(3)	0.0127(6)
	P_7(2.14)	1.00	0.7241(3)	0.0071(3)	0.2869(3)	0.0142(7)
	P_8(2.57)	1.00	0.7234(3)	0.0063(4)	0.2871(4)	0.0144(8)
	P_9(3.13)	1.00	0.7231(4)	0.0042(4)	0.2883 (4)	0.0178(9)
	P_{10}(3.92)	1.00	0.7212(5)	0.0003(6)	0.2891(6)	0.024(1)
	P_{11}(4.85)	1.00	0.7213(6)	-0.0050(8)	0.2923(7)	0.031(1)
	P_{21}(0.50)	1.00	0.7258(3)	0.0078(3)	0.2862(3)	0.0181(7)
T2(Si)	P_1(0.20)	1.00	0.4207(2)	0.1390(3)	0.0435(3)	0.0147(6)
	P_2(0.60)	1.00	0.4210(2)	0.1384(3)	0.0454(3)	0.0135(6)
	P_3(0.94)	1.00	0.4211(2)	0.1383(3)	0.0458(3)	0.0140(6)
	P_4(1.22)	1.00	0.4213(3)	0.1377(3)	0.0461(3)	0.0145(6)
	P_5(1.60)	1.00	0.4214(3)	0.1376(3)	0.0461(3)	0.0162(6)
	P_6(1.82)	1.00	0.4213(3)	0.1375(3)	0.0458(3)	0.0166(6)
	P_7(2.14)	1.00	0.4213(3)	0.1374(3)	0.0459(4)	0.0187(7)
	P_8(2.57)	1.00	0.4221(4)	0.1371(4)	0.0488(4)	0.0181(8)
	P_9(3.13)	1.00	0.4209(4)	0.1361(5)	0.0532(5)	0.0250(9)
	P_{10}(3.92)	1.00	0.4193(5)	0.1342(6)	0.0618(6)	0.032(1)
	P_{11}(4.85)	1.00	0.4167(7)	0.1308(9)	0.0725(8)	0.040(2)
	P_{21}(0.50)	1.00	0.4214(3)	0.1384(3)	0.0453(4)	0.0206(7)

Site	*P* (GPa)	*s.o.f.*	*x*	*y*	*z*	U_{iso}(Å^2)
T3(Si)	P_1(0.20)	1.00	0.0434(3)	0.0251(3)	0.2807(3)	0.0140(6)
	P_2(0.60)	1.00	0.0430(2)	0.0271(3)	0.2803(3)	0.0105(6)
	P_3(0.94)	1.00	0.0432(2)	0.0275(3)	0.2804(3)	0.0114(6)
	P_4(1.22)	1.00	0.0435(3)	0.0279(3)	0.2806(3)	0.0116(6)
	P_5(1.60)	1.00	0.0441(2)	0.0286(3)	0.2810(3)	0.0126(6)
	P_6(1.82)	1.00	0.0441(3)	0.0288(3)	0.2810(3)	0.0128(6)
	P_7(2.14)	1.00	0.0442(3)	0.0297(3)	0.2810(3)	0.0152(7)
	P_8(2.57)	1.00	0.0436(3)	0.0307(4)	0.2807(4)	0.0140(7)
	P_9(3.13)	1.00	0.0426(4)	0.0332(4)	0.2814(4)	0.0190(9)
	P_{10}(3.92)	1.00	0.0389(4)	0.0348(6)	0.2813(5)	0.023(1)
	P_{11}(4.85)	1.00	0.0352(6)	0.0396(8)	0.2816(8)	0.033(1)
	P_{21}(0.50)	1.00	0.0438(3)	0.0270(3)	0.2809(3)	0.0183(7)
T4(Si)	P_1(0.20)	1.00	0.0855(3)	0.1408(3)	0.0053(3)	0.0155(6)
	P_2(0.60)	1.00	0.0838(2)	0.1406(3)	0.0039(3)	0.0122(6)
	P_3(0.94)	1.00	0.0832(2)	0.1401(3)	0.0027(3)	0.0122(6)
	P_4(1.22)	1.00	0.0826(3)	0.1400(3)	0.0022(3)	0.0119(6)
	P_5(1.60)	1.00	0.0816(3)	0.1401(3)	0.0014(3)	0.0134(6)
	P_6(1.82)	1.00	0.0815(3)	0.1403(3)	0.0013(3)	0.0131(6)
	P_7(2.14)	1.00	0.0803(3)	0.1399(3)	0.0003(3)	0.0146(7)
	P_8(2.57)	1.00	0.0785(3)	0.1399(4)	-0.0014(4)	0.0140(8)
	P_9(3.13)	1.00	0.0750(4)	0.1398(4)	-0.0042(4)	0.0185(9)
	P_{10}(3.92)	1.00	0.0702(4)	0.1387(6)	-0.0090(5)	0.023(1)
	P_{11}(4.85)	1.00	0.0624(6)	0.1378(8)	-0.0176(7)	0.030(1)
	P_{21}(0.50)	1.00	0.0842(3)	0.1403(3)	0.0044(4)	0.0194(7)
O1	P_1(0.20)	1.00	0.0637(7)	0.1122(9)	0.1739(8)	0.027(2)
	P_2(0.60)	1.00	0.0625(7)	0.1160(8)	0.1738(8)	0.021(1)
	P_3(0.94)	1.00	0.0616(7)	0.1178(8)	0.1747(8)	0.020(1)
	P_4(1.22)	1.00	0.0628(7)	0.1187(8)	0.1763(9)	0.021(2)
	P_5(1.60)	1.00	0.0625(7)	0.1199(8)	0.1765(8)	0.023(1)
	P_6(1.82)	1.00	0.0633(7)	0.1197(8)	0.1772(9)	0.022(2)
	P_7(2.14)	1.00	0.0620(8)	0.1232(9)	0.1782(9)	0.024(2)
	P_8(2.57)	1.00	0.0598(9)	0.123(1)	0.175(1)	0.025(2)
	P_9(3.13)	1.00	0.051(1)	0.124(1)	0.170(1)	0.033(2)
	P_{10}(3.92)	1.00	0.036(1)	0.124(2)	0.155(2)	0.042(3)
	P_{11}(4.85)	1.00	0.024(2)	0.124(2)	0.149(2)	0.046(4)
	P_{21}(0.50)	1.00	0.0654(8)	0.1145(9)	0.1769(9)	0.028(2)

Site	P (GPa)	*s.o.f.*	x	y	z	U_{iso}(Å^2)
O2	P_1(0.20)	1.00	0.6325(8)	0.5868(9)	0.1517(9)	0.027(2)
	P_2(0.60)	1.00	0.6276(7)	0.5864(8)	0.1470(8)	0.025(1)
	P_3(0.94)	1.00	0.6262(7)	0.5844(9)	0.1470(8)	0.026(1)
	P_4(1.22)	1.00	0.6230(8)	0.585(1)	0.1441(9)	0.027(2)
	P_5(1.60)	1.00	0.6226(8)	0.5847(9)	0.1445(9)	0.027(2)
	P_6(1.82)	1.00	0.6215(8)	0.585(1)	0.144(1)	0.029(2)
	P_7(2.14)	1.00	0.6194(9)	0.584(1)	0.142(1)	0.030(2)
	P_8(2.57)	1.00	0.618(1)	0.583(1)	0.141(1)	0.030(2)
	P_9(3.13)	1.00	0.614(1)	0.585(1)	0.139(1)	0.036(2)
	P_{10}(3.92)	1.00	0.615(2)	0.588(2)	0.135(2)	0.054(3)
	P_{11}(4.85)	1.00	0.620(2)	0.585(3)	0.128(2)	0.069(5)
	P_{21}(0.50)	1.00	0.6272(9)	0.5849(9)	0.148(1)	0.033(2)
O3	P_1(0.20)	1.00	0.5951(8)	0.0981(9)	0.2257(9)	0.028(2)
	P_2(0.60)	1.00	0.5940(7)	0.0975(8)	0.2282(9)	0.027(2)
	P_3*(0.94)*	1.00	0.5952(7)	0.0971(8)	0.2305(8)	0.026(1)
	P_4(1.22)	1.00	0.5952(8)	0.0978(9)	0.2319(9)	0.026(2)
	P_5(1.60)	1.00	0.5962(8)	0.0989(9)	0.2333(9)	0.027(2)
	P_6(1.82)	1.00	0.5959(8)	0.0988(9)	0.233(1)	0.028(2)
	P_7(2.14)	1.00	0.5964(9)	0.099(1)	0.235(1)	0.030(2)
	P_8(2.57)	1.00	0.595(1)	0.099(1)	0.237(1)	0.031(2)
	P_9(3.13)	1.00	0.597(1)	0.094(1)	0.245(1)	0.038(2)
	P_{10}(3.92)	1.00	0.592(1)	0.086(2)	0.250(2)	0.044(3)
	P_{11}(4.85)	1.00	0.587(2)	0.080(2)	0.256(2)	0.042(4)
	P_{21}(0.50)	1.00	0.5964(9)	0.0962(9)	0.230(1)	0.036(2)
O4	P_1(0.20)	1.00	0.0371(8)	0.922(1)	0.1834(9)	0.029(2)
	P_2(0.60)	1.00	0.0359(7)	0.9267(9)	0.1792(9)	0.028(2)
	P_3(0.94)	1.00	0.0386(7)	0.9281(9)	0.1807(8)	0.026(1)
	P_4(1.22)	1.00	0.0404(8)	0.929(1)	0.181(1)	0.027(2)
	P_5(1.60)	1.00	0.0408(8)	0.930(1)	0.1798(9)	0.029(2)
	P_6(1.82)	1.00	0.0413(8)	0.929(1)	0.180(1)	0.029(2)
	P_7(2.14)	1.00	0.0439(9)	0.931(1)	0.181(1)	0.030(2)
	P_8(2.57)	1.00	0.045(1)	0.930(1)	0.182(1)	0.034(2)
	P_9(3.13)	1.00	0.047(1)	0.928(1)	0.185(1)	0.039(3)
	P_{10}(3.92)	1.00	0.054(2)	0.934(2)	0.191(2)	0.056(4)
	P_{11}(4.85)	1.00	0.061(2)	0.928(2)	0.212(2)	0.057(4)
	P_{21}(0.50)	1.00	0.0360(9)	0.925(1)	0.180(1)	0.037(2)

Site	P (GPa)	*s.o.f.*	x	y	z	U_{iso}(Å^2)
O5	P_1(0.20)	1.00	0.8765(7)	0.0448(8)	0.2738(8)	0.026(2)
	P_2(0.60)	1.00	0.8756(7)	0.0441(8)	0.2719(8)	0.023(1)
	P_3(0.94)	1.00	0.8762(7)	0.0451(8)	0.2734(8)	0.026(1)
	P_4(1.22)	1.00	0.8768(8)	0.0454(9)	0.2744(9)	0.026(2)
	P_5(1.60)	1.00	0.8749(8)	0.0456(9)	0.2723(9)	0.029(2)
	P_6(1.82)	1.00	0.8755(8)	0.0461(9)	0.273(1)	0.029(2)
	P_7(2.14)	1.00	0.8732(9)	0.045(1)	0.270(1)	0.034(2)
	P_8(2.57)	1.00	0.873(1)	0.046(1)	0.272(1)	0.032(2)
	P_9(3.13)	1.00	0.872(1)	0.045(1)	0.274(1)	0.043(3)
	P_{10}(3.92)	1.00	0.871(1)	0.048(2)	0.278(2)	0.047(3)
	P_{11}(4.85)	1.00	0.871(2)	0.046(2)	0.289(2)	0.053(4)
	P_{21}(0.50)	1.00	0.8756(8)	0.0470(9)	0.2730(9)	0.030(2)
O6	P_1(0.20)	1.00	0.2804(8)	0.3763(9)	0.0861(8)	0.028(1)
	P_2(0.60)	1.00	0.2804(7)	0.3778(8)	0.0876(9)	0.024(1)
	P_3(0.94)	1.00	0.2790(7)	0.3784(8)	0.0855(9)	0.024(1)
	P_4(1.22)	1.00	0.2785(8)	0.3793(9)	0.084(1)	0.026(2)
	P_5(1.60)	1.00	0.2766(8)	0.3789(9)	0.0824(9)	0.028(2)
	P_6(1.82)	1.00	0.2775(8)	0.3794(9)	0.084(1)	0.028(2)
	P_7(2.14)	1.00	0.2749(9)	0.380(1)	0.081(1)	0.030(1)
	P_8(2.57)	1.00	0.272(1)	0.381(1)	0.078(1)	0.030(2)
	P_9(3.13)	1.00	0.271(1)	0.383(1)	0.082(1)	0.040(3)
	P_{10}(3.92)	1.00	0.266(1)	0.388(2)	0.086(2)	0.045(3)
	P_{11}(4.85)	1.00	0.262(2)	0.393(2)	0.093(2)	0.049(4)
	P_{21}(0.50)	1.00	0.2808(9)	0.3764(9)	0.087(1)	0.036(2)
O7	P_1(0.20)	1.00	0.7934(7)	0.5203(8)	0.5026(7)	0.022(1)
	P_2(0.60)	1.00	0.7937(7)	0.5216(8)	0.5014(8)	0.022(1)
	P_3(0.94)	1.00	0.7938(7)	0.5224(8)	0.5021(8)	0.023(1)
	P_4(1.22)	1.00	0.7925(8)	0.5227(9)	0.5012(9)	0.024(2)
	P_5(1.60)	1.00	0.7925(8)	0.5243(9)	0.5013(9)	0.027(2)
	P_6(1.82)	1.00	0.7917(8)	0.5241(9)	0.501(1)	0.027(2)
	P_7(2.14)	1.00	0.7931(9)	0.526(1)	0.503(1)	0.032(2)
	P_8(2.57)	1.00	0.794(1)	0.529(1)	0.504(1)	0.033(2)
	P_9(3.13)	1.00	0.792(1)	0.535(1)	0.505(1)	0.040(2)
	P_{10}(3.92)	1.00	0.790(1)	0.543(2)	0.500(2)	0.042(3)
	P_{11}(4.85)	1.00	0.788(2)	0.554(2)	0.498(2)	0.049(4)
	P_{21}(0.50)	1.00	0.7941(8)	0.5229(9)	0.5024(9)	0.028(2)

Site	P (GPa)	*s.o.f.*	x	y	z	U_{iso}(Å^2)
O8	P_1(0.20)	0.50	0.550(1)	3/4	-0.019(1)	0.033(2)
	P_2(0.60)	0.50	0.551(1)	3/4	-0.019(1)	0.030(2)
	P_3(0.94)	0.50	0.552(1)	3/4	-0.018(1)	0.036(2)
	P_4(1.22)	0.50	0.554(1)	3/4	-0.017(1)	0.033(3)
	P_5(1.60)	0.50	0.557(1)	3/4	-0.014(2)	0.040(3)
	P_6(1.82)	0.50	0.556(1)	3/4	-0.014(2)	0.038(3)
	P_7(2.14)	0.50	0.558(2)	3/4	-0.011(2)	0.044(3)
	P_8(2.57)	0.50	0.554(2)	3/4	-0.017(2)	0.047(4)
	P_9(3.13)	0.50	0.552(2)	3/4	-0.029(2)	0.059(5)
	P_{10}(3.92)	0.50	0.545(3)	3/4	-0.050(3)	0.080(7)
	P_{11}(4.85)	0.50	0.546(4)	3/4	-0.069(5)	0.10(1)
	P_{21}(0.50)	0.50	0.550(1)	3/4	-0.020(1)	0.040(3)
O9	P_1(0.20)	0.50	0 .026(1)	1/4	-0.061(1)	0.029(2)
	P_2(0.60)	0.50	0.028(1)	1/4	-0.063(1)	0.026(2)
	P_3(0.94)	0.50	0.028(1)	1/4	-0.067(1)	0.027(2)
	P_4(1.22)	0.50	0.028(1)	1/4	-0.068(1)	0.025(2)
	P_5(1.60)	0.50	0.027(1)	1/4	-0.071(1)	0.028(2)
	P_6(1.82)	0.50	0.026(1)	1/4	0.071(1)	0.028(2)
	P_7(2.14)	0.50	0.026(1)	1/4	-0.073(1)	0.032(2)
	P_8(2.57)	0.50	0.023(1)	1/4	-0.079(2)	0.033(3)
	P_9(3.13)	0.50	0.022(2)	1/4	-0.084(2)	0.040(3)
	P_{10}(3.92)	0.50	0.017(2)	1/4	-0.097(3)	0.050(5)
	P_{11}(4.85)	0.50	0.022(3)	1/4	-0.097(4)	0.069(7)
	P_{21}(0.50)	0.50	0.026(1)	1/4	-0.064(1)	0.035(3)
K1	P_1(0.20)	0.59(2)	0.862(1)	1/4	0.226(2)	0.048(2)
	P_2(0.60)	0.49(2)	0.854(1)	1/4	0.220(1)	0.041(2)
	P_3(0.94)	0.46(2)	0.848(1)	1/4	0.215(2)	0.039(1)
	P_4(1.22)	0.44(2)	0.845(1)	1/4	0.212(3)	0.038(2)
	P_5(1.60)	0.42(3)	0.842(2)	1/4	0.209(3)	0.041(2)
	P_6(1.82)	0.42(3)	0.841(2)	1/4	0.208(3)	0.039(2)
	P_7(2.14)	0.50(4)	0.836(2)	1/4	0.199(3)	0.040(2)
	P_8(2.57)	0.51(4)	0.833(2)	1/4	0.199(3)	0.037(2)
	P_9(3.13)	0.50(4)	0.827(2)	1/4	0.197(4)	0.041(2)
	P_{10}(3.92)	0.48(4)	0.825(3)	1/4	0.208(5)	0.059(3)
	P_{11}(4.85)	0.53(7)	0.819(5)	1/4	0.211(8)	0.106(6)
	P_{21}(0.50)	0.51(2)	0.853(1)	1/4	0.217(2)	0.048(2)

Site	P (GPa)	*s.o.f.*	x	y	z	U_{iso}(Å^2)
K2	P_1(0.20)	0.33**	0.823(2)	1/4	0.152(3)	0.048(2)**
	P_2(0.60)	0.43**	0.817(1)	1/4	0.147(2)	0.041(2)**
	P_3(0.94)	0.46**	0.817(1)	1/4	0.147(2)	0.039(1)**
	P_4(1.22)	0.48**	0.816(1)	1/4	0.147(2)	0.038(2)**
	P_5(1.60)	0.50**	0.815(2)	1/4	0.148(3)	0.041(2)**
	P_6(1.82)	0.50**	0.811(2)	1/4	0.142(4)	0.040(2)**
	P_7(2.14)	0.42**	0.808(2)	1/4	0.139(4)	0.037(2)**
	P_8(2.57)	0.41**	0.808(2)	1/4	0.139(4)	0.037(2)**
	P_9(3.13)	0.42**	0.803(2)	1/4	0.137(4)	0.041(2)**
	P_{10}(3.92)	0.44**	0.797(3)	1/4	0.136(5)	0.059(3)**
	P_{11}(4.85)	0.39**	0.787*	1/4	0.135*	0.106(6)*
	P_{21}(0.50)	0.41**	0.814(2)	1/4	0.141(3)	0.048(2)**
W1	P_1(0.20)	0.62(4)	0.787(3)	1/4	0.530(3)	0.079(4)
	P_2(0.60)	0.32(4)	0.787(6)	1/4	0.531(7)	0.075*
	P_3(0.94)	0.21(4)	0.782(8)	1/4	0.54(1)	0.075*
	P_4(1.22)	0.17(4)	0.77(1)	1/4	0.56(1)	0.075*
	P_5(1.60)	0.20(4)	0.72(1)	1/4	0.56(1)	0.075*
	P_6(1.82)	0.16(4)	0.73(1)	1/4	0.56(1)	0.075*
	P_7(2.14)	0.19(4)	0.72(1)	1/4	0.55(1)	0.075*
	P_8(2.57)	0.30(5)	0.712(8)	1/4	0.559(9)	0.075*
	P_9(3.13)	0.46(5)	0.699(9)	1/4	0.550(7)	0.075*
	P_{10}(3.92)	0.35(5)	0.709(9)	1/4	0.568(9)	0.075*
	P_{11}(4.85)	0.36(6)	0.72(1)	1/4	0.57(1)	0.075*
	P_{21}(0.50)	0.42(3)	0.761(4)	1/4	0.582(5)	0.075*
W2	P_1(0.20)	0.60(4)	0.779(3)	3/4	0.430(3)	0.079(4)**
	P_2(0.60)	0.40(4)	0.791(5)	3/4	0.429(6)	0.075*
	P_3(0.94)	0.33(4)	0.792(7)	3/4	0.426(7)	0.075*
	P_4(1.22)	0.28(4)	0.798(8)	3/4	0.427(9)	0.075*
	P_5(1.60)	0.29(4)	0.791(8)	3/4	0.424(9)	0.075*
	P_6(1.82)	0.29(4)	0.788(8)	3/4	0.421(9)	0.075*
	P_7(2.14)	0.32(4)	0.791(7)	3/4	0.422(8)	0.075*
	P_8(2.57)	0.30(6)	0.72(1)	3/4	0.39(1)	0.075*
	P_9(3.13)	0.51(4)	0.670(5)	3/4	0.357(6)	0.075*
	P_{10}(3.92)	0.78(5)	0.659(4)	3/4	0.344(4)	0.075*
	P_{11}(4.85)	0.44(6)	0.65(1)	3/4	0.33(1)	0.075*
	P_{21}(0.50)	0.47(4)	0.761(4)	3/4	0.418(5)	0.075*

Site	*P* (GPa)	*s.o.f.*	*x*	*y*	*z*	U_{iso}(Å^2)
W3	P_1(0.20)	0.96(4)	0.342(1)	0.642(1)	0.158(1)	0.079(4)**
	P_2(0.60)	0.98(3)	0.342(1)	0.635(1)	0.156(2)	0.075*
	P_3(0.94)	0.98(3)	0.341(1)	0.632(1)	0.153(2)	0.075*
	P_4(1.22)	0.99(3)	0.341(1)	0.632(1)	0.154(2)	0.075*
	P_5(1.60)	0.99(3)	0.340(1)	0.631(1)	0.151(2)	0.075*
	P_6(1.82)	1.00*	0.340(1)	0.632(1)	0.153(2)	0.075*
	P_7(2.14)	1.00(3)	0.339(1)	0.630(2)	0.152(2)	0.075*
	P_8(2.57)	1.00*	0.342(2)	0.633(2)	0.158(2)	0.075*
	P_9(3.13)	0.98(3)	0.343(2)	0.636(2)	0.163(2)	0.075*
	P_{10}(3.92)	0.80(3)	0.343(2)	0.632(3)	0.162(3)	0.075*
	P_{11}(4.85)	0.69(4)	0.347(3)	0.631(4)	0.159(4)	0.075*
	P_{21}(0.50)	0.96(2)	0.347(1)	0.637(1)	0.163(2)	0.075*
W4	P_1(0.20)	0.55(4)	0.427(3)	1/4	0.437(3)	0.079(4)**
	P_2(0.60)	0.47(4)	0.426(4)	1/4	0.432(5)	0.075*
	P_3(0.94)	0.43(4)	0.421(4)	1/4	0.427(5)	0.075*
	P_4(1.22)	0.42(5)	0.422(5)	1/4	0.429(6)	0.075*
	P_5(1.60)	0.36(5)	0.419(6)	1/4	0.425(7)	0.075*
	P_6(1.82)	0.38(5)	0.418(5)	1/4	0.424(7)	0.075*
	P_7(2.14)	0.32(5)	0.419(7)	1/4	0.426(8)	0.075*
	P_8(2.57)	0.45(6)	0.417(6)	1/4	0.417(6)	0.075*
	P_9(3.13)	0.25(5)	0.41(1)	1/4	0.41(1)	0.075*
	P_{21}(0.50)	0.57(4)	0.423(3)	1/4	0.431(4)	0.075*
W5	P_1(0.20)	0.55(3)	0.526(3)	0.987(3)	0.545(3)	0.079(4)**
	P_2(0.60)	0.61(3)	0.534(2)	0.973(3)	0.545(3)	0.075*
	P_3(0.94)	0.60(3)	0.533(2)	0.975(3)	0.547(3)	0.075*
	P_4(1.22)	0.60(3)	0.536(2)	0.975(3)	0.547(3)	0.075*
	P_5(1.60)	0.60(3)	0.538(2)	0.976(3)	0.551(3)	0.075*
	P_6(1.82)	0.59(3)	0.536(2)	0.974(3)	0.547(3)	0.075*
	P_7(2.14)	0.62(3)	0.539(2)	0.977(3)	0.554(3)	0.075*
	P_8(2.57)	0.58(3)	0.538(3)	0.974(4)	0.552(4)	0.075*
	P_9(3.13)	0.51(3)	0.534(4)	0.977(4)	0.544(4)	0.075*
	P_{10}(3.92)	0.67(3)	0.533(3)	0.982(5)	0.536(4)	0.075*
	P_{11}(4.85)	0.68(4)	0.534(3)	1.021(5)	0.543(4)	0.075*
	P_{21}(0.50)	0.62(2)	0.531(2)	0.973(3)	0.542(3)	0.075*

Site	P (GPa)	*s.o.f.*	x	y	z	U_{iso}(Å^2)
W6	P_1(0.20)	0.29(2)	0.590(5)	0.870(6)	0.552(5)	0.079(4)**
	P_2(0.60)	0.41(3)	0.590(3)	0.856(4)	0.549(4)	0.075*
	P_3(0.94)	0.50(3)	0.589(3)	0.857(4)	0.544(3)	0.075*
	P_4(1.22)	0.56(3)	0.587(3)	0.856(4)	0.545(3)	0.075*
	P_5(1.60)	0.56(3)	0.590(3)	0.855(3)	0.546(3)	0.075*
	P_6(1.82)	0.59(3)	0.590(2)	0.856(3)	0.547(3)	0.075*
	P_7(2.14)	0.57(3)	0.591(3)	0.852(4)	0.547(3)	0.075*
	P_8(2.57)	0.56(3)	0.591(3)	0.857(4)	0.555(4)	0.075*
	P_9(3.13)	0.51**	0.593(4)	0.851(5)	0.545(4)	0.075*
	P_{10}(3.92)	0.52**	0.595(4)	0.844(4)	0.554(5)	0.075*
	P_{11}(4.85)	0.47**	0.609(5)	0.848(5)	0.566(6)	0.075*
	P_{21}(0.50)	0.46**	0.591(3)	0.863(4)	0.547(4)	0.075*
W2’	P_2(0.60)	0.29(3)	0.668(7)	3/4	0.369(8)	0.075*
	P_3(0.94)	0.34(7)	0.676(6)	3/4	0.376(7)	0.075*
	P_4(1.22)	0.36(4)	0.673(6)	3/4	0.374(8)	0.075*
	P_5(1.60)	0.33(4)	0.673(7)	3/4	0.376(8)	0.075*
	P_6(1.82)	0.34(4)	0.665(6)	3/4	0.370(8)	0.075*
	P_7(2.14)	0.37(4)	0.671(7)	3/4	0.368(8)	0.075*
	P_8(2.57)	0.40(6)	0.624(9)	3/4	0.346(8)	0.075*
W1’	P_9(3.13)	0.36(4)	0.005(7)	1/4	0.550(8)	0.075*
	P_{10}(3.92)	0.20(5)	0.02(1)	1/4	0.57(2)	0.075*
	P_{11}(4.85)	0.36(6)	0.051(9)	1/4	0.58(1)	0.075*
W2’’	P_{10}(3.92)	0.27(5)	0.46(1)	1/4	0.77(1)	0.075*
	P_{11}(4.85)	0.58(0)	0.446(8)	1/4	0.755(8)	0.075*

Table 4 (deposited). Refined T-O distances (Å) at different pressures.

P_n	P(GPa)	T1-O5	T1-O7	T1-O2	T1-O3	T2-O8	T2-O2	T2-O6	T2-O3
P_1	0.20(5)	1.635(1)	1.652(1)	1.661(2)	1.685(1)	1.634(2)	1.638(1)	1.644(1)	1.645(2)
P_2	0.60(5)	1.645(1)	1.637(1)	1.675 (2)	1.688(1)	1.642(2)	1.628(1)	1.645(1)	1.640(2)
P_3	0.94(5)	1.646(1)	1.643(1)	1.657(2)	1.668(1)	1.636(2)	1.645(1)	1.641(1)	1.650(2)
P_4	1.22(5)	1.647(1)	1.636(1)	1.679(2)	1.669(1)	1.641(2)	1.633(1)	1.637(1)	1.646(2)
P_5	1.60(5)	1.645(1)	1.639(1)	1.674(2)	1.678(1)	1.640(2)	1.630(1)	1.643(1)	1.650(2)
P_6	1.82(5)	1.649(1)	1.633(1)	1.673(2)	1.676(1)	1.641(2)	1.625(1)	1.641(1)	1.647(2)
P_7	2.14(5)	1.636(1)	1.647(1)	1.666(2)	1.666(1)	1.637(2)	1.618(1)	1.642(1)	1.651(2)
P_8	2.57(5)	1.633(1)	1.652(1)	1.656(2)	1.676(1)	1.637(2)	1.632(1)	1.638(1)	1.630(2)
P_9	3.13(5)	1.626(1)	1.662(1)	1.655(2)	1.643(1)	1.632(2)	1.641(1)	1.629(1)	1.665(2)
P_{10}	3.92(5)	1.655(1)	1.635(1)	1.651(1)	1.619(1)	1.650(2)	1.647(1)	1.645(1)	1.664(2)
P_{11}	4.85(5)	1.632(1)	1.628(1)	1.605(1)	1.639(1)	1.681(2)	1.657(1)	1.643(1)	1.654(1)
P_{21}	0.50(5)	1.647(1)	1.652(1)	1.668(2)	1.652(1)	1.643(2)	1.643(1)	1.638(1)	1.660(2)

P_n	P(GPa)	T3-O1	T3-O7	T3-O5	T3-O4	T4-O9	T4-O4	T4-O1	T4-O6
P_1	0.20(5)	1.622(1)	1.641(2)	1.642(1)	1.669(2)	1.637(2)	1.638(1)	1.650(1)	1.651(1)
P_2	0.60(5)	1.637(1)	1.650(1)	1.635(1)	1.651(2)	1.636(2)	1.641(1)	1.644(1)	1.664(1)
P_3	0.94(5)	1.639(1)	1.642(2)	1.635(1)	1.635(2)	1.641(2)	1.650(1)	1.653(1)	1.657(1)
P_4	1.22(5)	1.638(1)	1.650(2)	1.633(1)	1.631(2)	1.638(2)	1.655(2)	1.654(1)	1.657(1)
P_5	1.60(5)	1.640(1)	1.644(2)	1.643(1)	1.632(2)	1.638(2)	1.656(1)	1.657(1)	1.650(1)
P_6	1.82(5)	1.634(1)	1.649(2)	1.640(1)	1.644(2)	1.636(2)	1.649(1)	1.657(1)	1.657(1)
P_7	2.14(5)	1.644(2)	1.628(2)	1.639(1)	1.630(2)	1.636(2)	1.657(1)	1.659(1)	1.638(1)
P_8	2.57(5)	1.637(1)	1.619(2)	1.637(1)	1.651(2)	1.640(2)	1.637(1)	1.648(1)	1.634(1)
P_9	3.13(5)	1.611(1)	1.612(2)	1.633(1)	1.682(2)	1.634(2)	1.620(1)	1.655(1)	1.642(2)
P_{10}	3.92(5)	1.656(1)	1.656(2)	1.625(1)	1.634(2)	1.657(2)	1.657(1)	1.632(1)	1.633(1)
P_{11}	4.85(5)	1.576(1)	1.687(2)	1.633(1)	1.718(2)	1.643(2)	1.652(1)	1.672(1)	1.654(1)
P_{21}	0.50(5)	1.618(1)	1.637(2)	1.651(1)	1.666(2)	1.645(2)	1.633(1)	1.654(1)	1.662(1)

Table 5 (deposited). Refined distances (Å) at different pressures.

P_n	P(GPa)	K1-O1(x2)	K1-O8	K2-O1(x2)	K2-O8	Ca-O4	Ca-O7
P_1	0.20(5)	3.004(2)	3.391(3)	2.995(2)	3.181(2)	2.564(3)	2.642(2)
P_2	0.60(5)	2.995(2)	3.337(3)	2.981(2)	3.148(2)	2.541(3)	2.678(2)
P_3	0.94(5)	2.978(2)	3.300(3)	2.953(2)	3.148(2)	2.517(3)	2.707(3)
P_4	1.22(5)	2.976(2)	3.282(3)	2.948(2)	3.143(2)	2.493(3)	2.712(3)
P_5	1.60(5)	2.972(2)	3.283(3)	2.946(2)	3.153(2)	2.489(2)	2.747(3)
P_6	1.82(5)	2.981(2)	3.260(3)	2.941(2)	3.151(2)	2.474(2)	2.740(3)
P_7	2.14(5)	2.924(2)	3.226(2)	2.901(2)	3.118(2)	2.458(2)	2.771(3)
P_8	2.57(5)	2.927(2)	3.170(2)	2.894(2)	3.070(2)	2.440(2)	2.793(3)
P_9	3.13(5)	2.897(2)	3.109(2)	2.856(2)	3.027(2)	2.407(2)	2.867(3)
P_{10}	3.92(5)	2.908(2)	3.038(2)	2.827(2)	2.965(2)	2.419(2)	2.974(3)
P_{11}	4.85(5)	2.907(2)	3.025(2)	2.831(2)	2.952(1)	2.261(2)	3.048(3)
P_{21}	0.50(5)	3.008(2)	3.320(3)	3.016(2)	3.117(2)	2.591(3)	2.732(3)

P_n	P(GPa)	W1-Ca	W1-W6	W2-W6	W2-O8	W1-O9	W1-O3(x2)
P_1	0.20(5)	2.202(2)	3.790(2)	3.123(2)	3.207(3)	2.940(3)	3.081(3)
P_2	0.60(5)	2.174(2)	3.700(2)	3.104(1)	3.205(3)	2.923(3)	3.081(3)
P_3	0.94(5)	2.039(2)	3.613(2)	3.120(1)	3.175(3)	2.821(3)	3.121(3)
P_4	1.22(5)	1.879(2)	3.435(2)	3.164(1)	3.174(4)	2.753(4)	3.167(3)
P_5	1.60(5)	1.658(2)	3.059(2)	3.104(1)	3.129(3)	2.896(3)	3.161(2)
P_6	1.82(5)	1.653(1)	3.088(3)	3.096(1)	3.104(3)	2.842(3)	3.187(2)
P_7	2.14(5)	1.612(2)	2.980(2)	3.068(1)	3.085(3)	2.944(4)	3.092(2)
P_8	2.57(5)	1.565(2)	2.939(2)	2.809(3)	2.880(2)	2.860(3)	3.137(2)
P_9	3.13(5)	1.496(2)	2.844(2)	2.544(1)	2.826(2)	2.919(4)	3.087(2)
P_{10}	3.92(5)	1.512(2)	2.827(2)	2.563(1)	2.878(2)	2.720(3)	3.197(3)
P_{11}	4.85(5)	1.562(2)	2.986(2)	2.641(1)	2.938(2)	2.690(3)	3.229(3)
P_{21}	0.50(5)	2.114(2)	3.698(2)	2.958(2)	3.129(3)	2.957(3)	3.053(3)

Table 6. High-pressure evolution of the 8-mRs(001): relevant interatomic distances (Å), angles (°), and the ellipticity ratio $\varepsilon_{8\text{-mRs}(001)}$ (calculated as O5-O5/O9-O8, with O5-O5>O9-O8).

P_n	P(GPa)	O5-O5	O9-O8	O1-O1	O3-O3	O1-O3	$\varepsilon_{8\text{-mRs}(001)}$
P_1	0.20(5)	5.810(8)	6.121(2)	3.901(6)	4.299(6)	4.913(2)	0.948(2)
P_2	0.60(5)	5.828(8)	6.166(2)	3.794(5)	4.318(6)	4.929(2)	0.945(2)
P_3	0.94(5)	5.780(8)	6.180(2)	3.730(5)	4.314(6)	4.908(2)	0.935(2)
P_4	1.22(5)	5.756(8)	6.181(2)	3.693(5)	4.284(6)	4.907(2)	0.932(2)
P_5	1.60(5)	5.752(8)	6.203(2)	3.661(5)	4.252(6)	4.901(2)	0.927(2)
P_6	1.82(5)	5.731(8)	6.179(2)	3.661(5)	4.249(6)	4.899(2)	0.928(2)
P_7	2.14(5)	5.724(8)	6.161(2)	3.550(5)	4.233(6)	4.869(2)	0.929(2)
P_8	2.57(5)	5.706(8)	6.141(2)	3.532(5)	4.218(6)	4.869(2)	0.929(2)
P_9	3.13(5)	5.673(8)	6.194(2)	3.483(5)	4.316(6)	4.826(2)	0.915(2)
P_{10}	3.92(5)	5.555(8)	6.261(3)	3.465(5)	4.507(7)	4.849(2)	0.887(2)
P_{11}	4.85(5)	5.596(8)	6.431(3)	3.465(5)	4.678(7)	4.866(2)	0.870(2)
P_{21}	0.50(5)	5.747(8)	6.145(2)	3.836(5)	4.354(6)	4.924(2)	0.935(2)

P_n	P(GPa)	O1-O9-O1	O1-O5-O3	O5-O3-O8	O3-O8-O3
P_1	0.20(5)	92.90(5)	135.32(2)	116.62(3)	108.97(6)
P_2	0.60(5)	90.37(5)	134.76(2)	115.86(3)	108.84(7)
P_3	0.94(5)	88.20(5)	134.80(2)	115.62(3)	107.99(7)
P_4	1.22(5)	87.02(6)	134.71(2)	115.60(3)	106.92(7)
P_5	1.60(5)	85.93(5)	134.61(2)	115.84(2)	105.24(6)
P_6	1.82(5)	85.92(5)	134.89(2)	115.62(2)	105.40(7)
P_7	2.14(5)	83.56(5)	134.20(2)	115.17(2)	104.29(6)
P_8	2.57(5)	82.66(5)	133.92(2)	114.67(2)	105.55(6)
P_9	3.13(5)	81.13(5)	134.44(2)	113.40(3)	107.78(6)
P_{10}	3.92(5)	80.21(5)	136.65(3)	109.59(3)	114.45(7)
P_{11}	4.85(5)	79.23(4)	135.53(3)	109.20(3)	119.58(7)
P_{21}	0.50(5)	133.73(2)	137.03(3)	115.07(6)	109.09(6)

Table 7. High-pressure evolution of the 8-mRs[010]: relevant interatomic distances (Å), angles (°), and the ellipticity ratio $\varepsilon_{8\text{-mRs}[010]}$ (calculated as O3-O3/O1-O1, with O1-O1 > O3-O3).

P_n	P(GPa)	$\varepsilon_{8\text{-mRs}[010]}$	O6-O6	O7-O7	O1-O1	O3-O3
P_1	0.20(5)	0.852(5)	6.874(6)	5.810(2)	7.807(7)	6.652(3)
P_2	0.60(5)	0.838(5)	6.834(6)	5.833(2)	7.868(7)	6.592(3)
P_3	0.94(5)	0.831(5)	6.842(6)	5.818(2)	7.888(7)	6.553(3)
P_4	1.22(5)	0.829(5)	6.837(6)	5.789(2)	7.870(8)	6.528(3)
P_5	1.60(5)	0.828(5)	6.869(6)	5.793(2)	7.888(7)	6.532(3)
P_6	1.82(5)	0.829(5)	6.838(6)	5.775(2)	7.865(7)	6.522(3)
P_7	2.14(5)	0.820(5)	6.850(6)	5.762(2)	7.890(7)	6.466(3)
P_8	2.57(5)	0.811(5)	6.846(6)	5.758(2)	7.905(7)	6.409(3)
P_9	3.13(5)	0.777(5)	6.743(6)	5.725(2)	8.014(7)	6.230(3)
P_{10}	3.92(5)	0.729(5)	6.606(6)	5.762(2)	8.216(7)	5.986(3)
P_{11}	4.85(5)	0.687(5)	6.452(6)	5.801(2)	8.356(7)	5.737(2)
P_{21}	0.50(5)	0.844(5)	6.866(6)	5.833(2)	7.805(7)	6.590(3)

P_n	P(GPa)	O3-O7-O1	O7-O1-O6	O1-O6-O3	O6-O3-O7
P_1	0.20(5)	159.93(2)	107.69(2)	142.31(2)	124.73(2)
P_2	0.60(5)	159.38(2)	106.53(2)	142.82(2)	125.41(2)
P_3	0.94(5)	159.78(2)	106.10(2)	142.02(2)	125.74(2)
P_4	1.22(5)	159.75(3)	106.04(2)	141.39(2)	125.61(2)
P_5	1.60(5)	159.49(2)	106.15(2)	140.69(2)	125.42(2)
P_6	1.82(5)	159.51(2)	106.02(2)	140.98(2)	125.18(2)
P_7	2.14(5)	159.71(2)	105.57(2)	139.96(2)	125.63(2)
P_8	2.57(5)	158.78(2)	105.26(2)	139.31(2)	125.87(2)
P_9	3.13(5)	158.15(3)	101.97(2)	140.30(2)	126.64(2)
P_{10}	3.92(5)	154.43(3)	97.617(2)	143.43(3)	128.75(3)
P_{11}	4.85(5)	150.49(3)	93.749(2)	145.67(3)	130.10(3)
P_{21}	0.50(5)	159.19(2)	107.91(2)	141.50(2)	125.72(2)

Table 8. High-pressure evolution of the 8-mRs[100]-1: relevant interatomic distances (Å), angles (°), and the ellipticity ratio $\varepsilon_{8\text{-mRs}[100]\text{-}1}$ (calculated as O9-O8/O7-O7, with O7-O7 > O9-O8).

P_n	P(GPa)	O7-O7	O9-O8	O3-O3	O3-O4	O3-O8-O3	O4-O7-O3	$\varepsilon_{8\text{-mRs}[001]\text{-}1}$
P_1	0.20(5)	7.650(5)	6.669(7)	4.299(6)	4.288(5)	108.97(6)	38.50(2)	0.872(2)
P_2	0.60(5)	7.688(5)	6.657(7)	4.318(6)	4.306(5)	108.84(7)	38.27(2)	0.866(2)
P_3	0.94(5)	7.686(5)	6.635(7)	4.314(6)	4.274(5)	107.99(7)	37.98(2)	0.863(2)
P_4	1.22(5)	7.673(5)	6.638(8)	4.284(6)	4.262(5)	106.92(7)	37.93(2)	0.865(2)
P_5	1.60(5)	7.717(5)	6.650(7)	4.252(6)	4.261(5)	105.24(6)	37.76(2)	0.862(2)
P_6	1.82(5)	7.704(5)	6.637(7)	4.249(6)	4.258(5)	105.40(7)	37.82(2)	0.862(2)
P_7	2.14(5)	7.733(5)	6.621(7)	4.233(6)	4.219(5)	104.29(6)	37.39(2)	0.856(2)
P_8	2.57(5)	7.775(5)	6.515(7)	4.218(6)	4.192(5)	105.55(6)	37.16(2)	0.838(2)
P_9	3.13(5)	7.896(5)	6.385(7)	4.316(6)	4.089(4)	107.78(6)	35.97(2)	0.809(2)
P_{10}	3.92(5)	8.079(5)	6.133(7)	4.507(7)	3.999(4)	114.45(7)	34.35(2)	0.759(2)
P_{11}	4.85(5)	8.338(5)	6.007(7)	4.678(7)	3.817(4)	119.58(7)	32.38(2)	0.720(2)
P_{21}	0.50(5)	7.726(5)	6.640(7)	4.354(6)	4.285(5)	109.09(6)	38.03(2)	0.859(2)

Table 9. High-pressure evolution of the 8-mRs[100]-1: relevant interatomic distances (Å), angles (°), and the ellipticity ratio $\varepsilon_{8\text{-mRs}[100]\text{-}1}$ (calculated as O7-O7/O9-O8, with O9-O8 > O7-O7).

P_n	P(GPa)	O7-O7	O9-O8	O1-O9-O1	O7-O1-O9	O1-O7-O2	O2-O8-O2	$\varepsilon_{8\text{-mRs}[001]\text{-}1}$
P_1	0.20(5)	6.503(5)	7.794(6)	92.90(5)	156.53(2)	130.09(2)	124.44(8)	0.834(2)
P_2	0.60(5)	6.495(5)	7.820(6)	90.37(5)	157.16(2)	130.20(2)	125.64(8)	0.831(2)
P_3	0.94(5)	6.414(5)	7.835(6)	88.20(5)	157.57(1)	130.76(2)	126.30(8)	0.819(2)
P_4	1.22(5)	6.395(5)	7.837(7)	87.02(6)	158.06(3)	130.59(2)	127.12(9)	0.816(2)
P_5	1.60(5)	6.351(5)	7.832(6)	85.93(5)	158.13(2)	131.21(2)	127.92(8)	0.811(2)
P_6	1.82(5)	6.347(5)	7.827(6)	85.92(5)	158.44(2)	131.19(2)	128.07(9)	0.811(2)
P_7	2.14(5)	6.262(5)	7.798(6)	83.56(5)	158.89(2)	131.72(2)	129.45(8)	0.803(2)
P_8	2.57(5)	6.177(5)	7.866(6)	82.66(5)	158.66(2)	133.25(2)	127.98(8)	0.785(2)
P_9	3.13(5)	5.974(5)	7.955(6)	81.14(5)	154.94(2)	136.44(2)	124.53(7)	0.751(2)
P_{10}	3.92(5)	5.703(4)	8.163(7)	80.21(5)	149.88(3)	141.67(2)	119.02(7)	0.699(2)
P_{11}	4.85(5)	5.386(4)	8.318(7)	79.23(4)	143.77(3)	148.71(2)	116.21(7)	0.648(2)
P_{21}	0.50(5)	6.427(5)	7.831(6)	90.46(5)	157.60(2)	131.44(2)	125.70(8)	0.821(2)

Table 10. Refined elastic parameters of phillipsite for the first and the second compressional regime (see text for further details), based on II-BM equations of state fits. (*) fixed parameter; $K_0 = (1/\beta_{V,x})_{P0,T0} = -V(\partial P/\partial V)_{P0,T0}$; $K' = (\partial K/\partial P)_{T0}$

Elastic parameters of phillipsite in the first compressional regime (*P1-P6*)				
	V_0, l_0 (Å^3, Å)	K_0 (GPa)	K'	$\beta_{V,l}$ (GPa^{-1})
V	1005(1)	89(8)	4*	0.011(1)
a	9.914(7)	81(12)	4*	0.012(2)
b	14.201(9)	50(5)	4*	0.020(2)
c	8.707(2)	107(8)	4*	0.0093(7)
Elastic parameters of phillipsite in the second compressional regime (*P9-P20*)				
	V_0, x_0 (Å^3, Å)	K_0 (GPa)	K'	$\beta_{V,l}$ (GPa^{-1})
V	1098(2)	18.8(7)	4*	0.053(2)
a	10.07	30(2)	4*	0.033(2)
b	14.8(1)	11(1)	4*	0.091(8)
c	8.94(2)	21(1)	4*	0.048(2)

847

848 **Table 11.** Evolution of some selected T-O-T angles (°) with *P*.

849

P_n	*P*(GPa)	T4-O1-T3	T2-O8-T2	T1-O7-T3	T4-O6-T2
P_1	0.20(5)	144.74(4)	147.99(5)	144.38(3)	144.79(4)
P_2	0.60(5)	141.95(4)	148.39(5)	145.22(3)	143.87(4)
P_3	0.94(5)	139.95(4)	148.61(5)	144.95(3)	144.45(4)
P_4	1.22(5)	139.06(4)	148.76(9)	144.68(3)	144.53(4)
P_5	1.60(5)	138.28(4)	148.99(5)	144.39(3)	145.45(4)
P_6	1.82(5)	138.48(4)	148.79(9)	144.34(3)	144.59(4)
P_7	2.14(5)	135.34(4)	148.46(5)	144.18(3)	145.63(4)
P_8	2.57(5)	135.83(4)	148.46(5)	143.89(3)	146.20(4)
P_9	3.13(5)	135.58(4)	150.71(5)	140.88(3)	144.28(4)
P_{10}	3.92(5)	136.57(4)	150.65(5)	137.30(4)	141.34(4)
P_{11}	4.85(5)	137.37(4)	153.79(5)	132.80(4)	137.37(4)
P_{21}	0.50(5)	142.66(4)	148.03(5)	144.51(3)	145.10(4)

850

851

852

853

854

855

856

857

858

859

860

861

862

863

864

865

866

867

868

Figure 1. Configuration of the 8-mR[100]-1, 8mR[100]-2, 8-mR[010] and 8-mR(001) and of the extra-framework population in phillipsite (as viewed down [100]), based on the structural refinements at 0.20 GPa (*P*1).

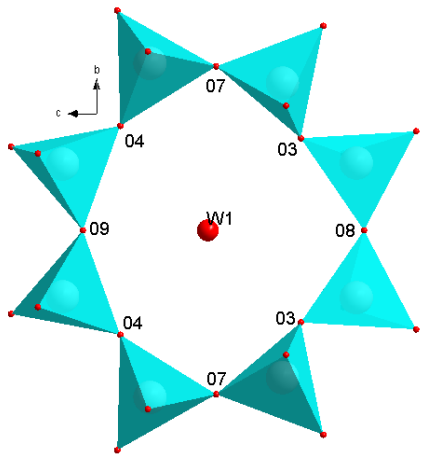

8-mRs[100]-1

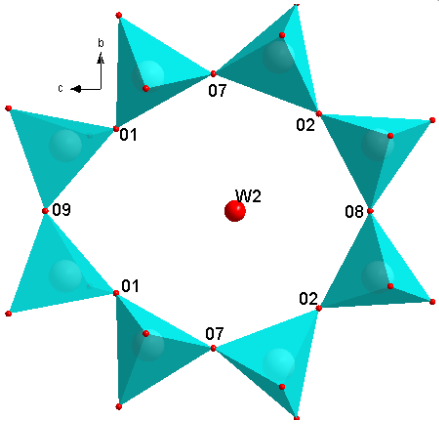

8-mRs[100]-2

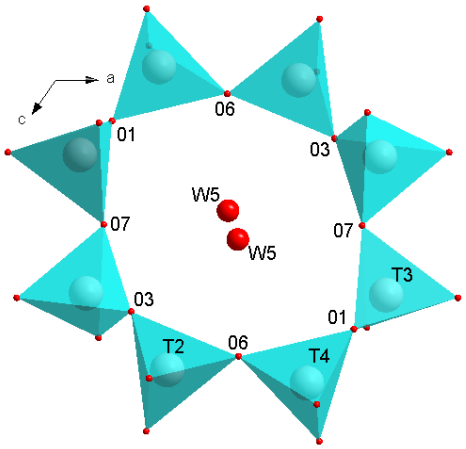

8-mRs[010]

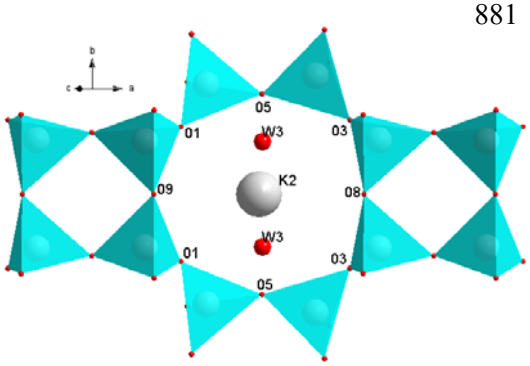

8-mRs(001)

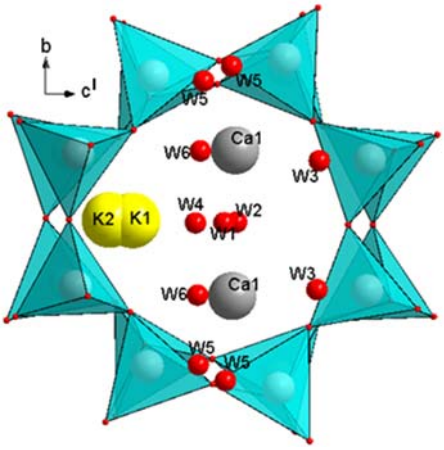

Configuration of the extra-framework population.

Figure 2. High-pressure evolution of the normalized (to *P*1) unit-cell volume and axial parameters of phillipsite compressed in *m.e.w.* V/V_0 in black squares, a/a_0 red circles, b/b_0 blue triangles, c/c_0 cyan triangles.

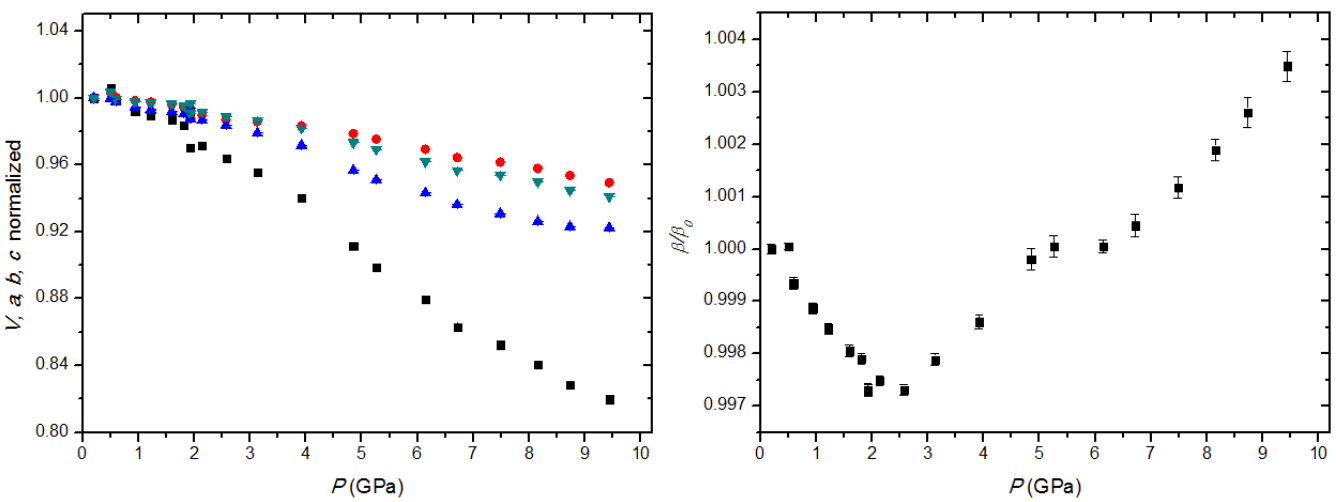

Figure 3. High-pressure evolution of some selected T-O-T angles. T2-O8-T2 in black squares, T1-O7-T3 red circles; T4-O1-T3 in black squares, T4-O6-T2 red circles.

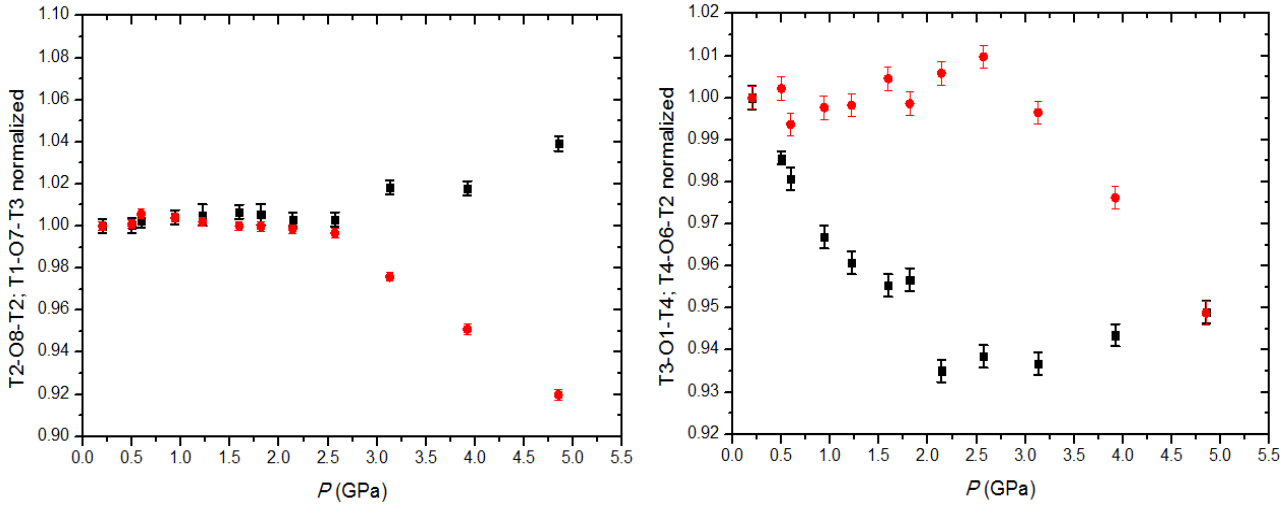

Figure 4. High-pressure evolution of the $\varepsilon_{8\text{-mRs}}$ parameters; $\varepsilon_{8\text{-mRs}}$[100]-1 in black squares, $\varepsilon_{8\text{-mRs}}$[100]-2 red circles, $\varepsilon_{8\text{-mRs}}$[010] blue triangle, and $\varepsilon_{8\text{-mRs}}$(001) cyan triangles.

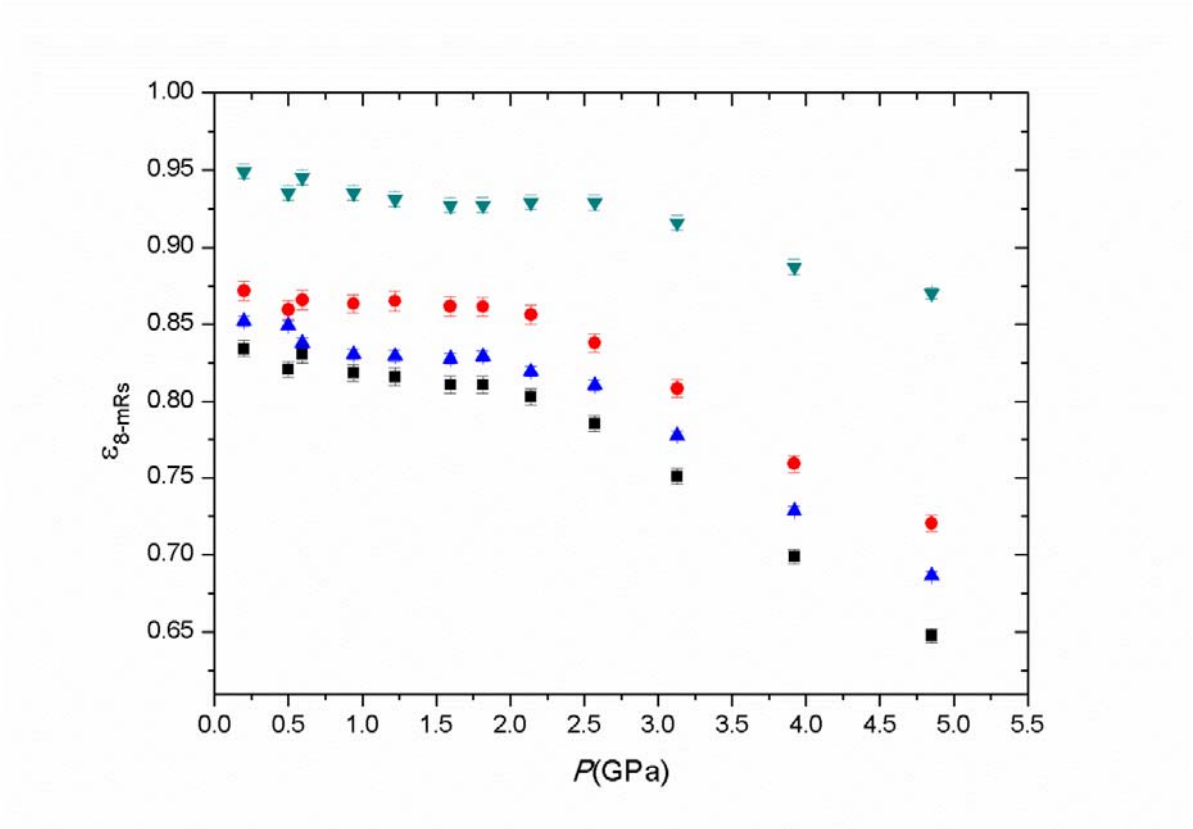

Figure 5. Evolution of the 8-mRs[010] diameters *vs*. pressure. O7-O7 in black squares, O3-O3 in red circles.

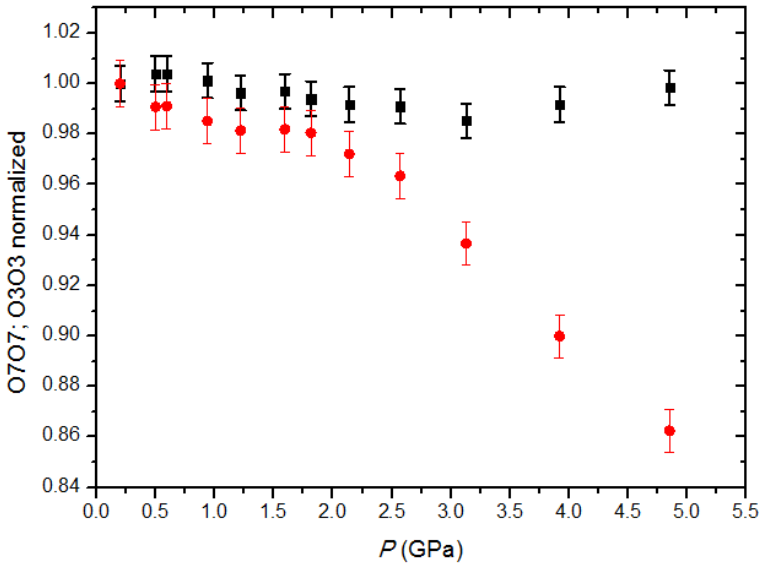

Figure 6. High-pressure evolution of the (normalized) difference between the inter-tetrahedral angles T3-O1-T4 and T4-O6-T2.

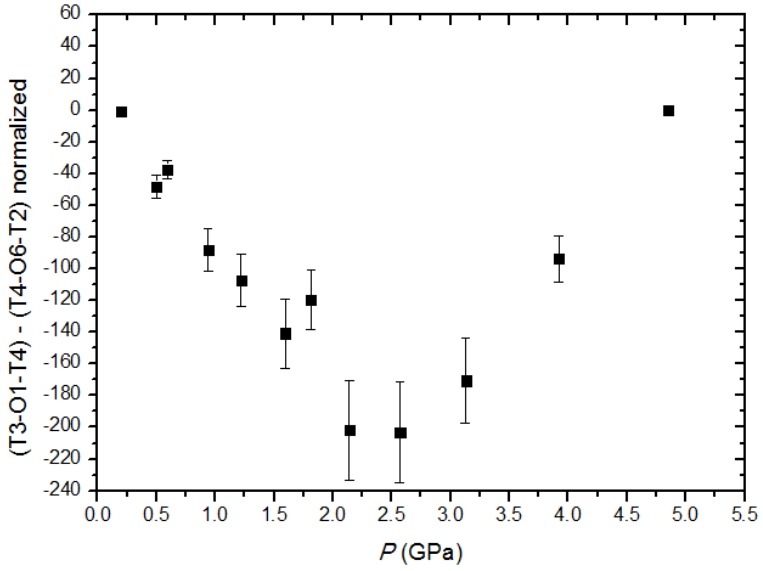

Figure 7. Migration of W1 with *P* viewed down [010] (*a,b,c*) and general view of the *P*-induced changes into the structure (*d,e*). H_2O molecules in small red spheres, K cations in yellow and Ca in dark grey.

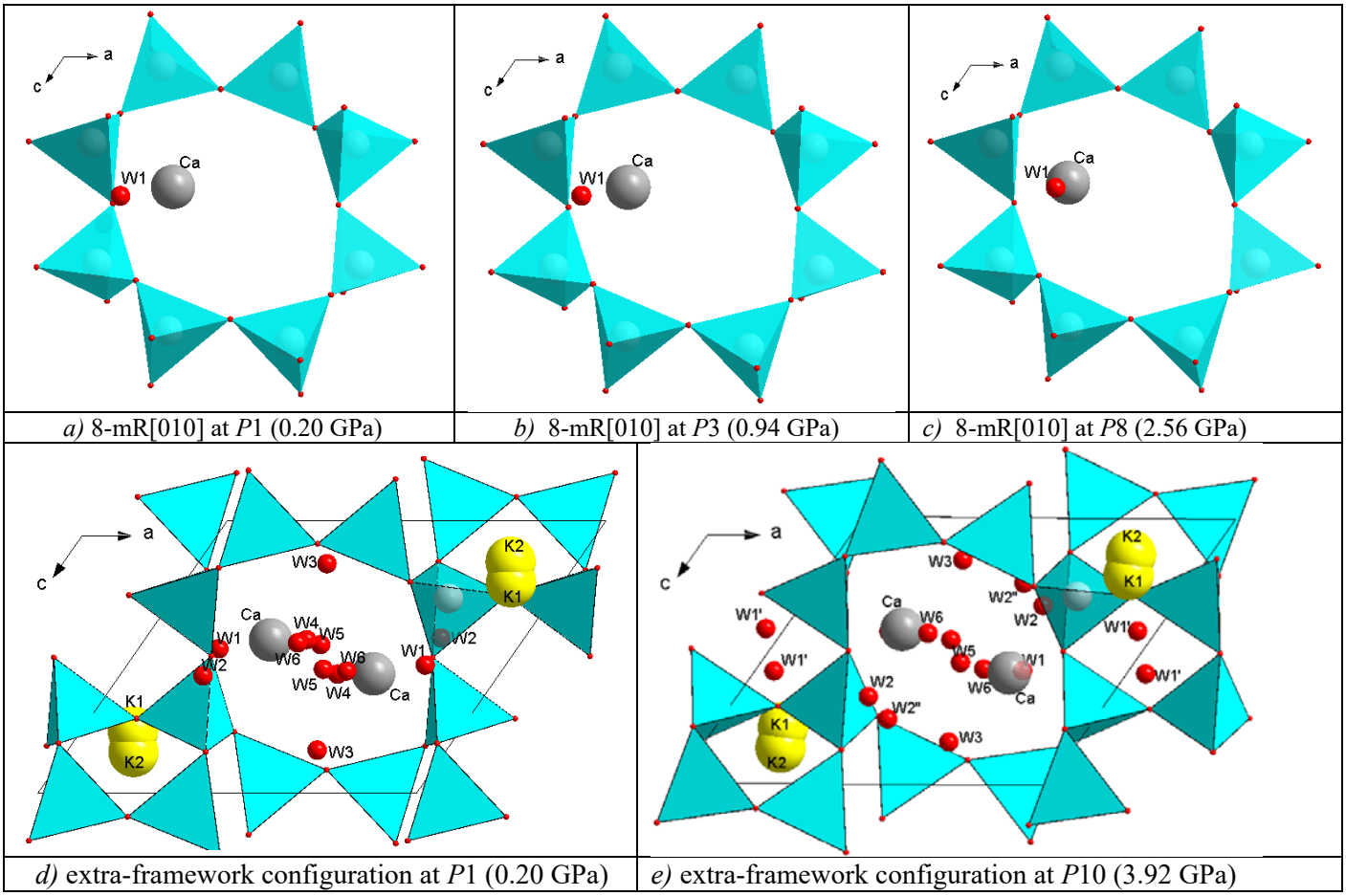

a) 8-mR[010] at *P*1 (0.20 GPa) | *b)* 8-mR[010] at *P*3 (0.94 GPa) | *c)* 8-mR[010] at *P*8 (2.56 GPa)

d) extra-framework configuration at *P*1 (0.20 GPa) | *e)* extra-framework configuration at *P*10 (3.92 GPa)

Figure 8. Clinographic view with the helicoidal configuration of the H_2O molecule-chain in the low (*left*) and high (*right*) compressional regime.